

Semileptonic B and B_s decays into orbitally excited charmed mesons

J. Segovia, C. Albertus, D.R. Entem, F. Fernández, E. Hernández, and M.A. Pérez-García

*Departamento de Física Fundamental e IUFFyM,
Universidad de Salamanca, E-37008 Salamanca, Spain*

(Dated: November 13, 2018)

The BaBar Collaboration has recently reported products of branching fractions that include B meson semileptonic decays into final states with charged and neutral $D_1(2420)$ and $D_2^*(2460)$, two narrow orbitally excited charmed mesons. We evaluate these branching fractions, together with those concerning $D_0^*(2400)$ and $D_1'(2430)$ mesons, within the framework of a constituent quark model. The calculation is performed in two steps, one of which involves a semileptonic decay and the other is mediated by a strong process. Our results are in agreement with the experimental data. We also extend the study to semileptonic decays of B_s into orbitally excited charmed-strange mesons, providing predictions to the possible measurements to be carried out at LHC.

PACS numbers: 12.39.Pn, 12.40.-y, 13.20.Fc

Keywords: potential models, models of strong interactions, leptonic and semileptonic decays

I. INTRODUCTION

Different collaborations have recently reported semileptonic B decays into orbitally excited charmed mesons providing detailed results of branching fractions. The theoretical analysis of these data, which include both weak and strong decays, offers the possibility for a stringent test of meson models.

Moreover, an accurate determination of the $|V_{cb}|$ and $|V_{ub}|$ Cabibbo-Kobayashi-Maskawa matrix elements demands a detailed knowledge of semileptonic decays of b -hadrons. Decays including orbitally excited charmed meson in the final state provide a substantial contribution to the total semileptonic decay width. Furthermore, a better understanding of these processes is also necessary in the analysis of signals and backgrounds of inclusive and exclusive measurements of b -hadron decays.

The Belle Collaboration [1], using a full reconstruction tagging method to suppress the large combinatorial background, reported data on the product of branching fractions $\mathcal{B}(B^+ \rightarrow D^{**}l^+\nu_l)\mathcal{B}(D^{**} \rightarrow D^{(*)}\pi)$, where, in the usual notation, l stands for a light e or μ lepton, the D_0^* , D_1' , D_1 and D_2^* mesons are denoted generically as D^{**} , and the D^* and D mesons as $D^{(*)}$.

D^{**} decays are reconstructed in the decay chains $D^{**} \rightarrow D^*\pi^\pm$ and $D^{**} \rightarrow D\pi^\pm$. In particular, the D_0^* meson decays only through the $D\pi$ channel, while the D_1' and D_1 mesons decay only via $D^*\pi$. Both $D\pi$ and $D^*\pi$ channels are opened in the case of D_2^* .

In the case of BaBar data [2, 3] the branching fractions $\mathcal{B}(D_2^* \rightarrow D^{(*)}\pi)$ include both the D^* and D contributions. As they also provide the ratio $\mathcal{B}_{D/D^{(*)}}$ we estimate the D^* and D contributions separately. The experimental results of both collaborations are given in Table I.

A similar analysis can be done in the strange sector for the B_s meson semileptonic decays. Here the intermediate states are the orbitally charmed-strange mesons, D_s^{**} , and the available final channels are DK and D^*K . The Particle Data Group (PDG) reports a value

$$\mathcal{B}(B_s^0 \rightarrow D_{s1}(2536)^-\mu^+\nu_\mu)\mathcal{B}(D_{s1}(2536)^- \rightarrow D^{*-}\bar{K}^0) = 2.4 \pm 0.7 [4] \text{ based on their best value for } \mathcal{B}(\bar{b} \rightarrow B_s^0) \text{ and the experimental data for } \mathcal{B}(\bar{b} \rightarrow B_s^0)\mathcal{B}(B_s^0 \rightarrow D_{s1}(2536)^-\mu^+\nu_\mu)\mathcal{B}(D_{s1}(2536)^- \rightarrow D^{*-}\bar{K}^0) \text{ measured by the D0 Collaboration [5].}$$

All these magnitudes can be consistently calculated in the framework of constituent quark models because they can simultaneously account for the hadronic part of the weak process and the strong meson decays. In this context, meson strong decay has been described successfully in phenomenological models, like the 3P_0 model [6] or the flux-tube model [7], or in microscopic models (see Refs. [8, 9]). The difference between the two approaches lies on the description of the $q\bar{q}$ creation vertex. While the 3P_0 model assumes that the $q\bar{q}$ pair is created from the vacuum with vacuum quantum numbers, in the microscopic model the $q\bar{q}$ pair is created from the interquark interactions already acting in the model. Both approaches will be used here to evaluate the strong decays. As for the weak process the matrix elements factorizes into a leptonic and a hadronic part. It is the hadronic part that contains the nonperturbative strong interaction effects and we shall evaluate it within a constituent quark model (CQM). We will work within the CQM of Ref. [10] which successfully describes hadron phenomenology and hadronic reactions [11–13] and has recently been applied to mesons containing heavy quarks in Refs. [14, 15].

The paper is organized as follows: In Sec. II we introduce the model we have used to get the masses and wave functions of the mesons involved in the reactions mentioned above. In Secs. III and IV we study the semileptonic and strong decay mechanisms, which constitute the two steps of the processes under study. Finally, we present our results in Sec. V and give some conclusions in Sec. VI.

	Belle [1] ($\times 10^{-3}$)	BaBar [2, 3] ($\times 10^{-3}$)
$D_0^*(2400)$		
$\mathcal{B}(B^+ \rightarrow \bar{D}_0^{*0} l^+ \nu_l) \mathcal{B}(\bar{D}_0^{*0} \rightarrow D^- \pi^+)$	$2.4 \pm 0.4 \pm 0.6$	$2.6 \pm 0.5 \pm 0.4$
$\mathcal{B}(B^0 \rightarrow D_0^{*-} l^+ \nu_l) \mathcal{B}(D_0^{*-} \rightarrow \bar{D}^0 \pi^-)$	$2.0 \pm 0.7 \pm 0.5$	$4.4 \pm 0.8 \pm 0.6$
$D_1'(2430)$		
$\mathcal{B}(B^+ \rightarrow \bar{D}_1'^0 l^+ \nu_l) \mathcal{B}(\bar{D}_1'^0 \rightarrow D^{*-} \pi^+)$	< 0.7	$2.7 \pm 0.4 \pm 0.5$
$\mathcal{B}(B^0 \rightarrow D_1'^- l^+ \nu_l) \mathcal{B}(D_1'^- \rightarrow \bar{D}^{*0} \pi^-)$	< 5	$3.1 \pm 0.7 \pm 0.5$
$D_1(2420)$		
$\mathcal{B}(B^+ \rightarrow \bar{D}_1^0 l^+ \nu_l) \mathcal{B}(\bar{D}_1^0 \rightarrow D^{*-} \pi^+)$	$4.2 \pm 0.7 \pm 0.7$	$2.97 \pm 0.17 \pm 0.17$
$\mathcal{B}(B^0 \rightarrow D_1^- l^+ \nu_l) \mathcal{B}(D_1^- \rightarrow \bar{D}^{*0} \pi^-)$	$5.4 \pm 1.9 \pm 0.9$	$2.78 \pm 0.24 \pm 0.25$
$D_2^*(2460)$		
$\mathcal{B}(B^+ \rightarrow \bar{D}_2^{*0} l^+ \nu_l) \mathcal{B}(\bar{D}_2^{*0} \rightarrow D^- \pi^+)$	$2.2 \pm 0.3 \pm 0.4$	$1.4 \pm 0.2 \pm 0.2^{(*)}$
$\mathcal{B}(B^+ \rightarrow \bar{D}_2^{*0} l^+ \nu_l) \mathcal{B}(\bar{D}_2^{*0} \rightarrow D^{*-} \pi^+)$	$1.8 \pm 0.6 \pm 0.3$	$0.9 \pm 0.2 \pm 0.2^{(*)}$
$\mathcal{B}(B^+ \rightarrow \bar{D}_2^{*0} l^+ \nu_l) \mathcal{B}(\bar{D}_2^{*0} \rightarrow D^{(*)-} \pi^+)$	$4.0 \pm 0.7 \pm 0.5$	$2.3 \pm 0.2 \pm 0.2$
$\mathcal{B}(B^0 \rightarrow D_2^{*-} l^+ \nu_l) \mathcal{B}(D_2^{*-} \rightarrow \bar{D}^0 \pi^-)$	$2.2 \pm 0.4 \pm 0.4$	$1.1 \pm 0.2 \pm 0.1^{(*)}$
$\mathcal{B}(B^0 \rightarrow D_2^{*-} l^+ \nu_l) \mathcal{B}(D_2^{*-} \rightarrow \bar{D}^{*0} \pi^-)$	< 3	$0.7 \pm 0.2 \pm 0.1^{(*)}$
$\mathcal{B}(B^0 \rightarrow D_2^{*-} l^+ \nu_l) \mathcal{B}(D_2^{*-} \rightarrow \bar{D}^{(*)0} \pi^-)$	< 5.2	$1.8 \pm 0.3 \pm 0.1$
$\mathcal{B}_{D/D^{(*)}}$	0.55 ± 0.03	$0.62 \pm 0.03 \pm 0.02$

TABLE I. Most recent experimental measurements reported by Belle and BaBar Collaborations. l stands for a light e or μ lepton. The symbol $(*)$ indicates results estimated from the original data by using $B_{D/D^{(*)}}$.

II. CONSTITUENT QUARK MODEL

Spontaneous chiral symmetry breaking of the QCD Lagrangian together with the perturbative one-gluon exchange (OGE) and the nonperturbative confining interaction are the main pieces of potential models. Using this idea, Vijande *et al.* [10] developed a model of the quark-quark interaction which is able to describe meson phenomenology from the light to the heavy quark sector. We briefly explain the model below. Further details can be found in Ref. [10].

One consequence of the spontaneous chiral symmetry breaking is that the nearly massless 'current' light quarks acquire a dynamical, momentum-dependent mass $M(p)$ with $M(0) \approx 300$ MeV for the u and d quarks, namely, the constituent mass. To preserve chiral invariance of the QCD Lagrangian new interaction terms, given by Goldstone boson exchanges, should appear between con-

stituent quarks.

A simple Lagrangian invariant under chiral transformations can be derived as [16]

$$\mathcal{L} = \bar{\psi}(i\gamma^\mu \partial_\mu - MU\gamma^5)\psi, \quad (1)$$

where $U\gamma^5 = \exp(i\pi^a \lambda^a \gamma^5 / f_\pi)$, π^a denotes the pseudoscalar fields ($\vec{\pi}, K, \eta_8$) and M is the constituent quark mass. The momentum-dependent mass acts as a natural cutoff of the theory. The chiral quark-quark interaction can be written as

$$V_{qq}(\vec{r}_{ij}) = V_{qq}^C(\vec{r}_{ij}) + V_{qq}^T(\vec{r}_{ij}) + V_{qq}^{SO}(\vec{r}_{ij}), \quad (2)$$

where C , T and SO stand for central, tensor and spin-orbit potentials. The central part presents four different contributions,

$$V_{qq}^C(\vec{r}_{ij}) = V_\pi^C(\vec{r}_{ij}) + V_\sigma^C(\vec{r}_{ij}) + V_K^C(\vec{r}_{ij}) + V_\eta^C(\vec{r}_{ij}), \quad (3)$$

given by

$$\begin{aligned}
V_\pi^C(\vec{r}_{ij}) &= \frac{g_{ch}^2}{4\pi} \frac{m_\pi^2}{12m_i m_j} \frac{\Lambda_\pi^2}{\Lambda_\pi^2 - m_\pi^2} m_\pi \left[Y(m_\pi r_{ij}) - \frac{\Lambda_\pi^3}{m_\pi^3} Y(\Lambda_\pi r_{ij}) \right] (\vec{\sigma}_i \cdot \vec{\sigma}_j) \sum_{a=1}^3 (\lambda_i^a \cdot \lambda_j^a), \\
V_\sigma^C(\vec{r}_{ij}) &= -\frac{g_{ch}^2}{4\pi} \frac{\Lambda_\sigma^2}{\Lambda_\sigma^2 - m_\sigma^2} m_\sigma \left[Y(m_\sigma r_{ij}) - \frac{\Lambda_\sigma}{m_\sigma} Y(\Lambda_\sigma r_{ij}) \right], \\
V_K^C(\vec{r}_{ij}) &= \frac{g_{ch}^2}{4\pi} \frac{m_K^2}{12m_i m_j} \frac{\Lambda_K^2}{\Lambda_K^2 - m_K^2} m_K \left[Y(m_K r_{ij}) - \frac{\Lambda_K^3}{m_K^3} Y(\Lambda_K r_{ij}) \right] (\vec{\sigma}_i \cdot \vec{\sigma}_j) \sum_{a=4}^7 (\lambda_i^a \cdot \lambda_j^a), \\
V_\eta^C(\vec{r}_{ij}) &= \frac{g_{ch}^2}{4\pi} \frac{m_\eta^2}{12m_i m_j} \frac{\Lambda_\eta^2}{\Lambda_\eta^2 - m_\eta^2} m_\eta \left[Y(m_\eta r_{ij}) - \frac{\Lambda_\eta^3}{m_\eta^3} Y(\Lambda_\eta r_{ij}) \right] (\vec{\sigma}_i \cdot \vec{\sigma}_j) [\cos \theta_p (\lambda_i^8 \cdot \lambda_j^8) - \sin \theta_p],
\end{aligned} \tag{4}$$

where $Y(x)$ is the standard Yukawa function defined by $Y(x) = e^{-x}/x$. We consider the physical η meson instead of the octet one and so we introduce the angle θ_p . The λ^a are the SU(3) flavor Gell-Mann matrices, m_i is the quark mass and m_π , m_K and m_η are the masses of the SU(3) Goldstone bosons, taken from experimental values. m_σ is determined through the PCAC relation $m_\sigma^2 \simeq m_\pi^2 + 4m_{u,d}^2$ [17]. Finally, the chiral coupling constant, g_{ch} , is determined from the πNN coupling constant through

$$\frac{g_{ch}^2}{4\pi} = \frac{9}{25} \frac{g_{\pi NN}^2}{4\pi} \frac{m_{u,d}^2}{m_N^2}, \tag{5}$$

which assumes that flavor SU(3) is an exact symmetry only broken by the different mass of the strange quark.

There are three different contributions to the tensor potential

$$V_{qq}^T(\vec{r}_{ij}) = V_\pi^T(\vec{r}_{ij}) + V_K^T(\vec{r}_{ij}) + V_\eta^T(\vec{r}_{ij}), \tag{6}$$

given by

$$\begin{aligned}
V_\pi^T(\vec{r}_{ij}) &= \frac{g_{ch}^2}{4\pi} \frac{m_\pi^2}{12m_i m_j} \frac{\Lambda_\pi^2}{\Lambda_\pi^2 - m_\pi^2} m_\pi \left[H(m_\pi r_{ij}) - \frac{\Lambda_\pi^3}{m_\pi^3} H(\Lambda_\pi r_{ij}) \right] S_{ij} \sum_{a=1}^3 (\lambda_i^a \cdot \lambda_j^a), \\
V_K^T(\vec{r}_{ij}) &= \frac{g_{ch}^2}{4\pi} \frac{m_K^2}{12m_i m_j} \frac{\Lambda_K^2}{\Lambda_K^2 - m_K^2} m_K \left[H(m_K r_{ij}) - \frac{\Lambda_K^3}{m_K^3} H(\Lambda_K r_{ij}) \right] S_{ij} \sum_{a=4}^7 (\lambda_i^a \cdot \lambda_j^a), \\
V_\eta^T(\vec{r}_{ij}) &= \frac{g_{ch}^2}{4\pi} \frac{m_\eta^2}{12m_i m_j} \frac{\Lambda_\eta^2}{\Lambda_\eta^2 - m_\eta^2} m_\eta \left[H(m_\eta r_{ij}) - \frac{\Lambda_\eta^3}{m_\eta^3} H(\Lambda_\eta r_{ij}) \right] S_{ij} [\cos \theta_p (\lambda_i^8 \cdot \lambda_j^8) - \sin \theta_p].
\end{aligned} \tag{7}$$

$S_{ij} = 3(\vec{\sigma}_i \cdot \hat{r}_{ij})(\vec{\sigma}_j \cdot \hat{r}_{ij}) - \vec{\sigma}_i \cdot \vec{\sigma}_j$ is the quark tensor operator and $H(x) = (1 + 3/x + 3/x^2)Y(x)$.

Finally, the spin-orbit potential only presents a contribution coming from the scalar part of the interaction

$$\begin{aligned}
V_{qq}^{\text{SO}}(\vec{r}_{ij}) &= V_\sigma^{\text{SO}}(\vec{r}_{ij}) = -\frac{g_{ch}^2}{4\pi} \frac{m_\sigma^3}{2m_i m_j} \frac{\Lambda_\sigma^2}{\Lambda_\sigma^2 - m_\sigma^2} \\
&\times \left[G(m_\sigma r_{ij}) - \frac{\Lambda_\sigma^3}{m_\sigma^3} G(\Lambda_\sigma r_{ij}) \right] (\vec{L} \cdot \vec{S}).
\end{aligned} \tag{8}$$

In the last equation $G(x)$ is the function $(1 + 1/x)Y(x)/x$.

Beyond the chiral symmetry breaking scale one expects

the dynamics to be governed by QCD perturbative effects. In this way one-gluon fluctuations around the instanton vacuum are taken into account through the qqg coupling

$$\mathcal{L}_{qqg} = i\sqrt{4\pi\alpha_s} \bar{\psi} \gamma_\mu G_c^\mu \lambda^c \psi, \tag{9}$$

with λ^c being the SU(3) color matrices and G_c^μ the gluon field.

The different terms of the potential derived from the Lagrangian contain central, tensor, and spin-orbit contributions and are given by

$$\begin{aligned}
V_{\text{OGE}}^{\text{C}}(\vec{r}_{ij}) &= \frac{1}{4} \alpha_s (\vec{\lambda}_i^c \cdot \vec{\lambda}_j^c) \left[\frac{1}{r_{ij}} - \frac{1}{6m_i m_j} (\vec{\sigma}_i \cdot \vec{\sigma}_j) \frac{e^{-r_{ij}/r_0(\mu)}}{r_{ij} r_0^2(\mu)} \right], \\
V_{\text{OGE}}^{\text{T}}(\vec{r}_{ij}) &= -\frac{1}{16} \frac{\alpha_s}{m_i m_j} (\vec{\lambda}_i^c \cdot \vec{\lambda}_j^c) \left[\frac{1}{r_{ij}^3} - \frac{e^{-r_{ij}/r_g(\mu)}}{r_{ij}} \left(\frac{1}{r_{ij}^2} + \frac{1}{3r_g^2(\mu)} + \frac{1}{r_{ij} r_g(\mu)} \right) \right] S_{ij}, \\
V_{\text{OGE}}^{\text{SO}}(\vec{r}_{ij}) &= -\frac{1}{16} \frac{\alpha_s}{m_i^2 m_j^2} (\vec{\lambda}_i^c \cdot \vec{\lambda}_j^c) \left[\frac{1}{r_{ij}^3} - \frac{e^{-r_{ij}/r_g(\mu)}}{r_{ij}^3} \left(1 + \frac{r_{ij}}{r_g(\mu)} \right) \right] \times \\
&\quad \times \left[(m_i + m_j)^2 + 2m_i m_j (\vec{S}_+ \cdot \vec{L}) + (m_j^2 - m_i^2) (\vec{S}_- \cdot \vec{L}) \right], \tag{10}
\end{aligned}$$

where $\vec{S}_{\pm} = \frac{1}{2}(\vec{\sigma}_i \pm \vec{\sigma}_j)$. Besides, $r_0(\mu) = \hat{r}_0 \frac{\mu_{nn}}{\mu_{ij}}$ and $r_g(\mu) = \hat{r}_g \frac{\mu_{nn}}{\mu_{ij}}$ are regulators which depend on μ_{ij} , the reduced mass of the $q\bar{q}$ pair. The contact term of the central potential has been regularized as

$$\delta(\vec{r}_{ij}) \sim \frac{1}{4\pi r_0^2} \frac{e^{-r_{ij}/r_0}}{r_{ij}} \tag{11}$$

The wide energy range needed to provide a consistent description of light, strange and heavy mesons requires an effective scale-dependent strong coupling constant. We use the frozen coupling constant of Ref. [10]

$$\alpha_s(\mu) = \frac{\alpha_0}{\ln\left(\frac{\mu^2 + \mu_0^2}{\Lambda_0^2}\right)}, \tag{12}$$

in which μ is the reduced mass of the $q\bar{q}$ pair and α_0 , μ_0 and Λ_0 are parameters of the model determined by a global fit to the meson spectra.

Confinement is one of the crucial aspects of QCD. Color charges are confined inside hadrons. It is well known that multigluon exchanges produce an attractive linearly rising potential proportional to the distance between quarks. This idea has been confirmed, but not rigorously proved, by quenched lattice gauge Wilson loop calculations for heavy valence quark systems. However, sea quarks are also important ingredients of the strong interaction dynamics. When included in the lattice calculations they contribute to the screening of the rising potential at low momenta and eventually to the breaking of the quark-antiquark binding string. This fact, which has been observed in $n_f = 2$ lattice QCD [18], has been taken into account in our model by including the terms

$$\begin{aligned}
V_{\text{CON}}^{\text{C}}(\vec{r}_{ij}) &= [-a_c(1 - e^{-\mu_c r_{ij}}) + \Delta] (\vec{\lambda}_i^c \cdot \vec{\lambda}_j^c), \\
V_{\text{CON}}^{\text{SO}}(\vec{r}_{ij}) &= -\left(\vec{\lambda}_i^c \cdot \vec{\lambda}_j^c\right) \frac{a_c \mu_c e^{-\mu_c r_{ij}}}{4m_i^2 m_j^2 r_{ij}} \left[((m_i^2 + m_j^2)(1 - 2a_s) + 4m_i m_j(1 - a_s)) (\vec{S}_+ \cdot \vec{L}) \right. \\
&\quad \left. + (m_j^2 - m_i^2)(1 - 2a_s) (\vec{S}_- \cdot \vec{L}) \right], \tag{13}
\end{aligned}$$

where a_s controls the mixture between the scalar and vector Lorentz structures of the confinement. At short distances this potential presents a linear behavior with an effective confinement strength $\sigma = -a_c \mu_c (\vec{\lambda}_i^c \cdot \vec{\lambda}_j^c)$ and becomes constant at large distances with a threshold defined by

$$V_{\text{thr}} = \{-a_c + \Delta\} (\vec{\lambda}_i^c \cdot \vec{\lambda}_j^c). \tag{14}$$

No $q\bar{q}$ bound states can be found for energies higher than this threshold. The system suffers a transition from a color string configuration between two static color sources into a pair of static mesons due to the breaking of the color string and the most favored decay into hadrons.

Among the different methods to solve the Schrödinger

equation in order to find the quark-antiquark bound states, we use the Gaussian Expansion Method [19] because it provides enough accuracy and it makes the subsequent evaluation of the decay amplitude matrix elements easier.

This procedure provides the radial wave function solution of the Schrödinger equation as an expansion in terms of basis functions

$$R_{\alpha}(r) = \sum_{n=1}^{n_{\text{max}}} c_n^{\alpha} \phi_{nl}^G(r), \tag{15}$$

where α refers to the channel quantum numbers. The coefficients, c_n^{α} , and the eigenvalue, E , are determined

Quark masses	m_n (MeV)	313
	m_s (MeV)	555
	m_c (MeV)	1763
	m_b (MeV)	5110
Goldstone Bosons	m_π (fm ⁻¹)	0.70
	m_σ (fm ⁻¹)	3.42
	m_K (fm ⁻¹)	2.51
	m_η (fm ⁻¹)	2.77
	Λ_π (fm ⁻¹)	4.20
	Λ_σ (fm ⁻¹)	4.20
	Λ_K (fm ⁻¹)	4.21
	Λ_η (fm ⁻¹)	5.20
	$g_{ch}^2/4\pi$	0.54
	θ_p (°)	-15
OGE	α_0	2.118
	Λ_0 (fm ⁻¹)	0.113
	μ_0 (MeV)	36.976
	\hat{r}_0 (fm)	0.181
	\hat{r}_g (fm)	0.259
Confinement	a_c (MeV)	507.4
	μ_c (fm ⁻¹)	0.576
	Δ (MeV)	184.432
	a_s	0.81

TABLE II. Quark model parameters.

from the Rayleigh-Ritz variational principle

$$\sum_{n=1}^{n_{max}} \left[(T_{n'n}^\alpha - EN_{n'n}^\alpha) c_n^\alpha + \sum_{\alpha'} V_{n'n}^{\alpha\alpha'} c_n^{\alpha'} = 0 \right], \quad (16)$$

where $T_{n'n}^\alpha$, $N_{n'n}^\alpha$ and $V_{n'n}^{\alpha\alpha'}$ are the matrix elements of the kinetic energy, the normalization and the potential, respectively. $T_{n'n}^\alpha$ and $N_{n'n}^\alpha$ are diagonal whereas the mixing between different channels is given by $V_{n'n}^{\alpha\alpha'}$.

Following Ref. [19], we employ Gaussian trial functions with ranges in geometric progression. This enables the optimization of ranges employing a small number of free parameters. Moreover, the geometric progression is dense at short distances, so that it allows the description of the dynamics mediated by short range potentials. The fast damping of the gaussian tail is not a problem, since we can choose the maximal range much longer than the hadronic size.

Table II shows the model parameters fitted over all meson spectra and taken from Refs. [10, 14].

III. WEAK DECAYS

In this section, we give an account of the semileptonic decays of the B (B or B_s) meson into orbitally

excited charmed mesons. In the nonstrange sector, this has been studied before within heavy quark effective theory (HQET) in Refs. [20, 21]. There, only relative branching ratios could be predicted and their results depended on the approximation used and on two unknown functions, τ_1 , τ_2 , that describe corrections of order Λ_{QCD}/m_Q . Only the ratio $\Gamma_{D^{**}}^{\lambda=0}/\Gamma_{D^{**}}$, semileptonic decay rate with a helicity 0 D^{**} final meson over total semileptonic decay rate to that meson, seemed to be stable in the different approximations. We shall comment on this below.

In the context of nonrelativistic constituent quark models, the state of a meson is given by

$$|M, \lambda \vec{P}\rangle_{NR} = \int \frac{d^3p}{(2\pi)^{3/2}} \sum_{\alpha_1, \alpha_2} \frac{(-1)^{1/2-s_1}}{\sqrt{2E_{f_1}(\vec{p}_1)2E_{f_2}(\vec{p}_2)}} \times \hat{\phi}_{\alpha_1, \alpha_2}^{(M, \lambda)}(\vec{p}) | \bar{q}, \alpha_1 \vec{p}_1 \rangle | q, \alpha_2 \vec{p}_2 \rangle, \quad (17)$$

where \vec{P} is the three-momentum of the meson and λ is the spin projection in the meson center of mass. The vector \vec{p} is the relative momentum of the $q\bar{q}$ pair, $\vec{p}_1 = \frac{m_{f_1}}{m_{f_1}+m_{f_2}}\vec{P}-\vec{p}$ and $\vec{p}_2 = \frac{m_{f_2}}{m_{f_1}+m_{f_2}}\vec{P}+\vec{p}$ are the momenta of the antiquark and the quark, respectively, α_1 and α_2 are the spin, flavor and color quantum numbers. $(E(\vec{p}_i), \vec{p}_i)$ are the four-momenta and m_i are the quark masses. The factor $(-1)^{1/2-s_1}$ is included in order that the antiquark spin states have the correct relative phase.

The normalization of the quark-antiquark states is

$$\langle \alpha' \vec{p}' | \alpha \vec{p} \rangle = \delta_{\alpha', \alpha} (2\pi)^3 2E_f(\vec{p}) \delta(\vec{p}' - \vec{p}), \quad (18)$$

and the momentum space wave function $\hat{\phi}_{\alpha_1, \alpha_2}^{(M, \lambda)}(\vec{p})$ normalization is given by

$$\int d^3p \sum_{\alpha_1, \alpha_2} (\hat{\phi}_{\alpha_1, \alpha_2}^{(M, \lambda')}(\vec{p}))^* \hat{\phi}_{\alpha_1, \alpha_2}^{(M, \lambda)}(\vec{p}) = \delta_{\lambda', \lambda}. \quad (19)$$

Finally, the normalization of our meson states is

$${}_{NR} \langle M, \lambda' \vec{P}' | M, \lambda \vec{P} \rangle_{NR} = \delta_{\lambda', \lambda} (2\pi)^3 \delta(\vec{P}' - \vec{P}). \quad (20)$$

In the decay we have a $\bar{b} \rightarrow \bar{c}$ transition at the quark level and we need to evaluate the hadronic matrix elements of the weak current

$$J_\mu^{bc}(0) = \bar{\psi}_b(0) \gamma_\mu (I - \gamma_5) \psi_c(0). \quad (21)$$

The hadronic matrix elements can be parameterized in terms of form factors as

$$\begin{aligned}
\langle D(0^+), \lambda \vec{P}_D | J_\mu^{bc}(0) | B(0^-), \vec{P}_B \rangle &= P_\mu F_+(q^2) + q_\mu F_-(q^2), \\
\langle D(1^+), \lambda \vec{P}_D | J_\mu^{bc}(0) | B(0^-), \vec{P}_B \rangle &= \frac{-1}{m_B + m_D} \epsilon_{\mu\nu\alpha\beta} \epsilon_{(\lambda)}^{\nu*}(\vec{P}_D) P^\alpha q^\beta A(q^2) \\
&\quad - i \left\{ (m_B - m_D) \epsilon_{(\lambda)\mu}^*(\vec{P}_D) V_0(q^2) - \frac{P \cdot \epsilon_{(\lambda)}^*(\vec{P}_D)}{m_B + m_D} [P_\mu V_+(q^2) + q_\mu V_-(q^2)] \right\}, \quad (22) \\
\langle D(2^+), \lambda \vec{P}_D | J_\mu^{bc}(0) | B(0^-), \vec{P}_B \rangle &= \epsilon_{\mu\nu\alpha\beta} \epsilon_{(\lambda)}^{\nu\delta*}(\vec{P}_D) P_\delta P^\alpha q^\beta T_4(q^2) \\
&\quad - i \left\{ \epsilon_{(\lambda)\mu\delta}^*(\vec{P}_D) P^\delta T_1(q^2) + P^\nu P^\delta \epsilon_{(\lambda)\nu\delta}^*(\vec{P}_D) [P_\mu T_2(q^2) + q_\mu T_3(q^2)] \right\}.
\end{aligned}$$

In the expressions above, $P = P_B + P_D$ and $q = P_B - P_D$, P_B and P_D being the meson four-momenta. m_B and m_D are the meson masses, $\epsilon^{\mu\nu\alpha\beta}$ is the fully antisymmetric tensor, for which the convention $\epsilon^{0123} = +1$ is taken, and $\epsilon_{(\lambda)\mu}(\vec{P})$ and $\epsilon_{(\lambda)\mu\nu}(\vec{P})$ are the polarization vector and tensor of vector and tensor mesons, respectively. The meson states in the Lorentz decompositions of Eq. (22) are normalized such that

$$\langle M, \lambda' \vec{P}' | M, \lambda \vec{P} \rangle = \delta_{\lambda'\lambda} (2\pi)^3 2E_M(\vec{P}) \delta(\vec{P}' - \vec{P}). \quad (23)$$

where $E_M(\vec{P})$ is the energy of the M meson with three-momentum \vec{P} . Note the factor $2E_M$ difference with respect to Eq. (20).

The form factors will be evaluated in the center of mass

of the 0^- meson, taking \vec{q} in the \hat{z} direction, so that $\vec{P}_B = \vec{0}$ and $\vec{P}_D = -\vec{q} = -|\vec{q}|\vec{k}$, with \vec{k} representing the unit vector in the \hat{z} direction. We have taken the phases of the states such that all form factors are real. F_+ , F_- , A , V_0 , V_+ , V_- and T_1 are dimensionless, whereas T_2 , T_3 and T_4 have dimension of E^{-2} . Defining vector $V_\lambda^\mu(|\vec{q}|)$ and axial $A_\lambda^\mu(|\vec{q}|)$ matrix elements such that

$$\begin{aligned}
V_\lambda^\mu(|\vec{q}|) &= \langle M_F, \lambda - |\vec{q}|\vec{k} | J_V^{bc\mu}(0) | M_I, \vec{0} \rangle, \\
A_\lambda^\mu(|\vec{q}|) &= \langle M_F, \lambda - |\vec{q}|\vec{k} | J_A^{bc\mu}(0) | M_I, \vec{0} \rangle, \quad (24)
\end{aligned}$$

we have for a $0^- \rightarrow 0^+$ decay, that the form factors are given in terms of vector and axial matrix elements as

$$\begin{aligned}
F_+(q^2) &= \frac{-1}{2m_B} \left[A^0(|\vec{q}|) + \frac{A^3(|\vec{q}|)}{|\vec{q}|} (E_D(-\vec{q}) - m_B) \right], \\
F_-(q^2) &= \frac{-1}{2m_B} \left[A^0(|\vec{q}|) + \frac{A^3(|\vec{q}|)}{|\vec{q}|} (E_D(-\vec{q}) + m_B) \right].
\end{aligned} \quad (25)$$

In the case of a $0^- \rightarrow 1^+$ transition, the corresponding

expressions for the form factors are

$$\begin{aligned}
A(q^2) &= -\frac{i}{\sqrt{2}} \frac{m_B + m_D}{m_B |\vec{q}|} A_{\lambda=-1}^1(|\vec{q}|), \\
V_+(q^2) &= +i \frac{m_B + m_D}{2m_B} \frac{m_D}{|\vec{q}| m_B} \left\{ V_{\lambda=0}^0(|\vec{q}|) - \frac{m_B - E_D(-\vec{q})}{|\vec{q}|} V_{\lambda=0}^3(|\vec{q}|) + \sqrt{2} \frac{m_B E_D(-\vec{q}) - m_D^2}{|\vec{q}| m_D} V_{\lambda=-1}^1(|\vec{q}|) \right\}, \\
V_-(q^2) &= -i \frac{m_B + m_D}{2m_B} \frac{m_D}{|\vec{q}| m_B} \left\{ -V_{\lambda=0}^0(|\vec{q}|) - \frac{m_B + E_D(-\vec{q})}{|\vec{q}|} V_{\lambda=0}^3(|\vec{q}|) + \sqrt{2} \frac{m_B E_D(-\vec{q}) + m_D^2}{|\vec{q}| m_D} V_{\lambda=-1}^1(|\vec{q}|) \right\}, \\
V_0(q^2) &= +i \sqrt{2} \frac{1}{m_B - m_D} V_{\lambda=-1}^1(|\vec{q}|).
\end{aligned} \quad (26)$$

Finally, the form factors for a $0^- \rightarrow 2^+$ transition are

given by the relations

$$\begin{aligned}
T_1(q^2) &= -i \frac{2m_D}{m_B |\vec{q}|} A_{T\lambda=+1}^1(|\vec{q}|), \\
T_2(q^2) &= i \frac{1}{2m_B^3} \left\{ -\sqrt{\frac{3}{2}} \frac{m_D^2}{|\vec{q}|^2} A_{T\lambda=0}^0(|\vec{q}|) - \sqrt{\frac{3}{2}} \frac{m_D^2}{|\vec{q}|^3} (E_D(-\vec{q}) - m_B) A_{T\lambda=0}^3(|\vec{q}|) \right. \\
&\quad \left. + \frac{2m_D}{|\vec{q}|} \left(1 - \frac{E_D(-\vec{q})(E_D(-\vec{q}) - m_B)}{|\vec{q}|^2} \right) A_{T\lambda=+1}^1(|\vec{q}|) \right\}, \\
T_3(q^2) &= i \frac{1}{2m_B^3} \left\{ -\sqrt{\frac{3}{2}} \frac{m_D^2}{|\vec{q}|^2} A_{T\lambda=0}^0(|\vec{q}|) - \sqrt{\frac{3}{2}} \frac{m_D^2}{|\vec{q}|^3} (E_D(-\vec{q}) + m_B) A_{T\lambda=0}^3(|\vec{q}|) \right. \\
&\quad \left. + \frac{2m_D}{|\vec{q}|} \left(1 - \frac{E_D(-\vec{q})(E_D(-\vec{q}) + m_B)}{|\vec{q}|^2} \right) A_{T\lambda=+1}^1(|\vec{q}|) \right\}, \\
T_4(q^2) &= i \frac{m_D}{m_B^2 |\vec{q}|^2} V_{T\lambda=+1}^1(|\vec{q}|). \tag{27}
\end{aligned}$$

The CQM evaluation of the vector and axial matrix elements $V_\lambda^\mu(|\vec{q}|)$ and $A_\lambda^\mu(|\vec{q}|)$ can be found in the Appendix.

For a B meson at rest and neglecting the neutrino mass, we have the double differential decay width

$$\begin{aligned}
\frac{d^2\Gamma}{dq^2 dx_l} &= \frac{G_F^2}{64m_B^2} \frac{|V_{bc}|^2}{8\pi^3} \frac{\lambda^{1/2}(q^2, m_B^2, m_D^2)}{2m_B} \frac{q^2 - m_l^2}{q^2} \\
&\quad \times \mathcal{H}_{\alpha\beta}(P_B, P_D) \mathcal{L}^{\alpha\beta}(p_l, p_\nu), \tag{28}
\end{aligned}$$

where x_l is the cosine of the angle between the final meson momentum and the momentum of the final charged lepton measured in the lepton-neutrino center of mass frame. $G_F = 1.16637(1) \times 10^{-5} \text{ GeV}^{-2}$ is the Fermi constant [4], m_l is the charged lepton mass, $\lambda(a, b, c) = (a + b - c)^2 - 4ab$ and V_{bc} is the bc element of the Cabibbo-Kobayashi-Maskawa matrix for which we shall use $V_{bc} = 0.0413$. $\mathcal{H}_{\alpha\beta}$ and $\mathcal{L}^{\alpha\beta}$ represent the hadron and lepton tensors. P_B, P_D, p_l and p_ν are the meson and lepton momenta.

Working in the helicity formalism of Ref. [22] and after integration on x_l we have

$$\begin{aligned}
\frac{d\Gamma}{dq^2} &= \frac{G_F^2}{8\pi^3} |V_{bc}|^2 \frac{(q^2 - m_l^2)^2}{12m_B^2 q^2} \frac{\lambda^{1/2}(q^2, m_B^2, m_D^2)}{2m_B} \\
&\quad \times (H_U + H_L + \tilde{H}_U + \tilde{H}_L + \tilde{H}_S), \tag{29}
\end{aligned}$$

where the suffixes U, L, S stand for the unpolarized-transverse, longitudinal and scalar components of the hadronic tensor, and $\tilde{H} = \frac{m_l^2}{2q^2} H$. Integrating over q^2 we obtain the total decay width that can be written as

$$\Gamma = \Gamma_U + \Gamma_L + \tilde{\Gamma}_U + \tilde{\Gamma}_L + \tilde{\Gamma}_S, \tag{30}$$

with Γ_J and $\tilde{\Gamma}_J$ partial helicity widths defined as

$$\Gamma_J = \int dq^2 \frac{G_F^2}{8\pi^3} |V_{bc}|^2 \frac{(q^2 - m_l^2)^2}{12m_B^2 q^2} \frac{\lambda^{1/2}(q^2, m_B^2, m_D^2)}{2m_B} H_J \tag{31}$$

and similarly for $\tilde{\Gamma}_J$ in terms of \tilde{H}_J . The evaluation of the different form factors, and thus of the different helicity amplitudes of the hadronic tensor, has been done following Ref. [23].

IV. STRONG DECAYS

Meson strong decay is a complex nonperturbative process that has not yet been described from QCD first principles. Instead, several phenomenological models have been developed to deal with this topic, the 3P_0 [6], the flux-tube [7], and the Cornell [8, 9] models being the most popular.

Some models describe the decay process assuming that the extra quark-antiquark pair is created from the vacuum. This is the case of the 3P_0 model, which borrows its name from the quantum numbers of the created pair, or the flux-tube model, which in addition to the creation vertex incorporates the overlaps between the color flux tubes of the initial and final states.

To address a more fundamental description of the decay mechanism, one has to describe hadron strong decays in terms of quark and gluon degrees of freedom. However, there has been little previous work in this area. Two different examples are the study of open-charm decays of $c\bar{c}$ resonances by Eichten *et al.* [8], who assumed that the decays are due to pair production from the static part of a Lorentz vector confining interaction, and the study of a few strong decays in the light sector by Ackleh *et al.* [9], where the $q\bar{q}$ pair production comes from the one-gluon exchange and a scalar confining interaction.

As we mentioned in the introduction, we shall use both the 3P_0 model and a microscopic one, resembling those of Refs. [8] and [9], that originates from the different interaction pieces present in our interquark potential. These two approaches to meson production are introduced in the following subsections.

A. The 3P_0 model

It was first proposed by Micu [6] and further developed by Le Yaouanc *et al.* [24]. To describe the meson decay process $A \rightarrow B + C$, the 3P_0 model assumes that a quark-antiquark pair is created with vacuum $J^{PC} = 0^{++}$ quantum numbers. The created $q\bar{q}$ pair together with the $q\bar{q}$ pair present in the original meson regroup in the two outgoing mesons via a quark rearrangement process.

The interaction Hamiltonian which describes the production process is given by [9]

$$H_I = g \int d^3x \bar{\psi}(\vec{x}) \psi(\vec{x}) \quad (32)$$

where g is related to the dimensionless constant giving the strength of the $q\bar{q}$ pair creation from the vacuum as $\gamma = \frac{g}{2m_q}$, m_q being the mass of the created quark. Note that the operator $g\bar{\psi}\psi$ leads to the decay $(q\bar{q})_A \rightarrow (q\bar{q})_B + (q\bar{q})_C$ through the $a^\dagger b^\dagger$ term.

B. The microscopic model

In microscopic decay models one attempts to describe hadron strong decays in terms of quark and gluon degrees

- Currents

$$J(\vec{x}) = \bar{\psi}(\vec{x}) \Gamma \psi(\vec{x}) = \begin{cases} \bar{\psi}(\vec{x}) \mathcal{I} \psi(\vec{x}) & \text{Scalar Lorentz current,} \\ \bar{\psi}(\vec{x}) \gamma^0 \psi(\vec{x}) & \text{Static part of vector Lorentz current,} \\ \bar{\psi}(\vec{x}) \vec{\gamma} \psi(\vec{x}) & \text{Spatial part of vector Lorentz current,} \end{cases} \quad (34)$$

- Kernels

$$K(r) = \begin{cases} -4a_s [-a_c(1 - e^{-\mu_c r}) + \Delta] & \text{Confining interaction,} \\ +\frac{\alpha_s}{r} & \text{Color Coulomb OGE,} \\ -\frac{\alpha_s}{r} & \text{Transverse OGE.} \end{cases} \quad (35)$$

For the Lorentz vector structure of the confinement we use $K(r) = \pm(1 - a_s)4[-a_c(1 - e^{-\mu_c r}) + \Delta]$, where \pm refers to static and transverse terms, respectively. We refer, following Ref. [9], to this general type of interaction as a JKJ decay model, and to the specific cases considered here as sKs , j^0Kj^0 and j^TKj^T interactions.

The wave functions for the mesons involved in the reactions are the solutions of the Schrödinger equation using the Gaussian Expansion Method mentioned above. Details of the resulting matrix elements for different cases are given in Ref. [25].

of freedom. The quark-gluon decay mechanism should give similar predictions to the reasonably accurate 3P_0 model and should determine the strength of the $q\bar{q}$ pair creation, γ , of the 3P_0 model in terms of more fundamental parameters.

Following Ref. [9], the strong decays should be driven by the same interquark Hamiltonian which determines the spectrum, the one-gluon exchange, and the confining interaction appearing as the kernels. These interactions and their associated decay amplitudes are undoubtedly all present and should be added coherently. We already mentioned that our constituent quark model for the heavy quark sector has a one-gluon exchange term and a mixture of Lorentz scalar and vector confining interactions. This completely defines our microscopic model for strong decays. Unlike previous works we use a screening confinement interaction and also a mixture between scalar and vector Lorentz structures, which is already fixed.

The Hamiltonian of the interaction can be written as

$$H_I = \frac{1}{2} \int d^3x d^3y J^a(\vec{x}) K(|\vec{x} - \vec{y}|) J^a(\vec{y}). \quad (33)$$

The current J^a in Eq. (33) is assumed to be a color octet. The currents, J , with the color dependence $\lambda^a/2$ factored out and the kernels, $K(r)$, for the interactions are

C. Strong decay width

The total width is the sum over the partial widths characterized by the quantum numbers J_{BC} and l

$$\Gamma_{A \rightarrow BC} = \sum_{J_{BC}, l} \Gamma_{A \rightarrow BC}(J_{BC}, l) \quad (36)$$

where

$$\Gamma_{A \rightarrow BC}(J_{BC}, l) = 2\pi \int dk_0 \delta(E_A - E_{BC}) |\mathcal{M}_{A \rightarrow BC}(k_0)|^2 \quad (37)$$

and $\mathcal{M}_{A \rightarrow BC}(k_0)$ is calculated according to Refs. [25, 26].

Using relativistic phase space, we arrive at

$$\Gamma_{A \rightarrow BC}(J_{BC}, l) = 2\pi \frac{E_B E_C}{m_A k_0} |\mathcal{M}_{A \rightarrow BC}(k_0)|^2, \quad (38)$$

where

$$k_0 = \frac{\lambda^{1/2}(m_A^2, m_B^2, m_C^2)}{2m_A} \quad (39)$$

is the on shell relative momentum of mesons B and C .

V. RESULTS

For the low-lying positive parity excitations, any quark model predicts four states that in the $^{2S+1}L_J$ basis correspond to 1P_1 , 3P_0 , 3P_1 and 3P_2 . As charge conjugation is not well defined in the heavy-light sector, 1P_1 and 3P_1 states can mix under the interaction.

In the infinite heavy quark mass limit, heavy quark symmetry (HQS) predicts two degenerated P -wave meson doublets, labeled by $j_q = 1/2$ with $J^P = 0^+, 1^+$ ($|1/2, 0^+\rangle, |1/2, 1^+\rangle$) and $j_q = 3/2$ with $J^P = 1^+, 2^+$ ($|3/2, 1^+\rangle, |3/2, 2^+\rangle$). In this limit, the meson properties are governed by the dynamics of the light quark, which is characterized by its total angular momentum $j_q = s_q + L$, where s_q is the light quark spin and L the orbital angular momentum. The total angular momentum of the meson J is obtained coupling j_q to the heavy quark spin, s_Q .

Moreover, in the infinite heavy quark mass limit the strong decays of the D_J ($j_q = 3/2$) proceed only through D -waves, while the D_J ($j_q = 1/2$) decays happen only through S -waves [27]. The D -wave decay is suppressed by the barrier factor which behaves as q^{2L+1} where q is the relative momentum of the two decaying mesons. Therefore, the states decaying through D -waves are expected to be narrower than those decaying via S -waves.

A change of basis allows to express the above states in terms of the $^{2S+1}L_J$ basis, by recoupling angular momenta, as

$$\begin{aligned} |1/2, 0^+\rangle &= +|^3P_0\rangle \\ |1/2, 1^+\rangle &= +\sqrt{\frac{1}{3}}|^1P_1\rangle + \sqrt{\frac{2}{3}}|^3P_1\rangle \\ |3/2, 1^+\rangle &= -\sqrt{\frac{2}{3}}|^1P_1\rangle + \sqrt{\frac{1}{3}}|^3P_1\rangle \\ |3/2, 2^+\rangle &= +|^3P_2\rangle \end{aligned} \quad (40)$$

where in the $^{2S+1}L_J$ wave functions we couple heavy and light quark spins, in this order, to total spin S .

In the actual calculation the ideal mixing in Eq. (40) between 1P_1 and 3P_1 states changes due to finite charm quark mass effects. Our CQM model predicts the mixed states shown in Table III, which are very similar to the HQS states. This is expected since the c -quark is much heavier ($m_c = 1763$ MeV) than the light ($m_n = 313$ MeV) or strange ($m_s = 555$ MeV) quarks. Note that now we

	D_0^*	D_1	D_1'	D_2^*
3P_0	+, 1.0000	-	-	-
1P_1	-	-, 0.5903	-, 0.4097	-
3P_1	-	+, 0.4097	-, 0.5903	-
3P_2	-	-	-	+, 0.99993
$1/2, 0^+$	+, 1.0000	-	-	-
$1/2, 1^+$	-	+, 0.0063	-, 0.9937	-
$3/2, 1^+$	-	+, 0.9937	+, 0.0063	-
$3/2, 2^+$	-	-	-	+, 0.99993
	D_{s0}^*	D_{s1}	D_{s1}'	D_{s2}^*
3P_0	+, 1.0000	-	-	-
1P_1	-	-, 0.7210	-, 0.1880	-
3P_1	-	+, 0.2770	-, 0.5570	-
3P_2	-	-	-	+, 0.99991
$1/2, 0^+$	+, 1.0000	-	-	-
$1/2, 1^+$	-	-, 0.0038	-, 0.7390	-
$3/2, 1^+$	-	+, 0.9942	-, 0.0060	-
$3/2, 2^+$	-	-	-	+, 0.99991

TABLE III. Probability distributions and their relative phases for the four states predicted by CQM in the two basis described in the text. In the 1^+ strange sector the effects of non- $q\bar{q}$ components are included, see text for details.

have mixing, even if small, between the 3P_2 and 3F_2 partial waves in 2^+ mesons. This is due to the OGE tensor term.

In Ref. [15] we have studied the $J^P = 1^+$ charmed-strange mesons, finding that the $J^P = 1^+$ $D_{s1}(2460)$ has an important non- $q\bar{q}$ contribution whereas the $J^P = 1^+$ $D_{s1}(2536)$ is almost a pure $q\bar{q}$ state. The presence of non- $q\bar{q}$ degrees of freedom in the $J^P = 1^+$ charmed-strange meson sector enhances the $j_q = 3/2$ component of the $D_{s1}(2536)$. This wave function explains most of the experimental data, as shown in Ref. [15], and it is the one we shall use here. For this sector only the $q\bar{q}$ probabilities are given in Table III.

A. B semileptonic decays into D^{**} mesons

1. Semileptonic $B \rightarrow D_0^*(2400)l\nu_l$ decay

The measured branching fractions are $\mathcal{B}(B^+ \rightarrow \bar{D}_0^{*0}l^+\nu_l)\mathcal{B}(\bar{D}_0^{*0} \rightarrow D^-\pi^+)$ and $\mathcal{B}(B^0 \rightarrow D_0^{*-}l^+\nu_l)\mathcal{B}(D_0^{*-} \rightarrow \bar{D}^0\pi^-)$. The meson $D_0^*(2400)$ has $J^P = 0^+$ quantum numbers and, therefore, due to parity conservation, it decays only into $D\pi$, so that we have $\mathcal{B}(\bar{D}_0^{*0} \rightarrow D^-\pi^+) = \mathcal{B}(D_0^{*-} \rightarrow \bar{D}^0\pi^-) = 2/3$ coming from isospin symmetry.

Table IV shows the different helicity contributions to the semileptonic width. In both cases the dominant contribution is given by Γ_L while the rest are negligible. The difference between the semileptonic width of the charged

	$B^+ \rightarrow \bar{D}_0^{*0} l^+ \nu_l$	$B^0 \rightarrow D_0^{*-} l^+ \nu_l$
Γ_U	0.00	0.00
$\tilde{\Gamma}_U$	0.00	0.00
Γ_L	1.30	1.16
$\tilde{\Gamma}_L$	6.83×10^{-7}	6.45×10^{-7}
$\tilde{\Gamma}_S$	2.05×10^{-6}	1.93×10^{-6}
Γ	1.30	1.16

TABLE IV. Helicity contributions and total decay widths, in units of 10^{-15} GeV, for the D_0^* meson.

	$B^+ \rightarrow \bar{D}'_1{}^0 l^+ \nu_l$	$B^0 \rightarrow D'_1{}^- l^+ \nu_l$
Γ_U	0.23	0.23
$\tilde{\Gamma}_U$	1.35×10^{-8}	1.35×10^{-8}
Γ_L	0.56	0.56
$\tilde{\Gamma}_L$	4.12×10^{-7}	4.12×10^{-7}
$\tilde{\Gamma}_S$	1.27×10^{-6}	1.27×10^{-6}
Γ	0.79	0.80

TABLE V. Helicity contributions and total decay widths, in units of 10^{-15} GeV, for the D'_1 meson.

and neutral B meson is due to the large mass difference between the D_0^* and $D_0^{*\pm}$ mesons for which we take the masses reported in Ref. [4].

Figure 1 shows the q^2 dependence in the form factors and in the differential decay width for $\mathcal{B}(B^+ \rightarrow \bar{D}_0^{*0} l^+ \nu_l)$, panels (a) and (b), respectively. Similar results (not shown) are obtained for the $\mathcal{B}(B^0 \rightarrow D_0^{*-} l^+ \nu_l)$ case.

The final results for the product of branching fractions are

$$\begin{aligned} \mathcal{B}(B^+ \rightarrow \bar{D}_0^{*0} l^+ \nu_l) \mathcal{B}(\bar{D}_0^{*0} \rightarrow D^- \pi^+) &= 2.15 \times 10^{-3}, \\ \mathcal{B}(B^0 \rightarrow D_0^{*-} l^+ \nu_l) \mathcal{B}(D_0^{*-} \rightarrow \bar{D}^0 \pi^-) &= 1.80 \times 10^{-3}, \end{aligned} \quad (41)$$

which compare very well with Belle data [1].

2. Semileptonic $B \rightarrow D'_1(2430) l \nu_l$ decay

The only Okubo-Zweig-Iizuka (OZI)-allowed decay channel for the D'_1 meson is $D'_1 \rightarrow D^* \pi$ so that isospin symmetry predicts a branching fraction $\mathcal{B}(D'_1 \rightarrow D^* \pi^\pm) = 2/3$.

Table V shows the different helicity contributions to the semileptonic width of $B^+ \rightarrow \bar{D}'_1{}^0 l^+ \nu_l$ and $B^0 \rightarrow D'_1{}^- l^+ \nu_l$ calculated in the framework of the CQM. In this case, Γ_U and Γ_L are of the same order of magnitude and give the total semileptonic decay rate.

Panels (a) and (b) of Fig. 2 show the q^2 dependence of the form factors and the differential decay width for the neutral D'_1 channel. A very similar result is obtained for the D_0^* case.

	$B^+ \rightarrow D_1^0 l^+ \nu_l$	$B^0 \rightarrow D_1^- l^+ \nu_l$
Γ_U	0.38	0.38
$\tilde{\Gamma}_U$	1.94×10^{-8}	1.93×10^{-8}
Γ_L	1.17	1.16
$\tilde{\Gamma}_L$	7.16×10^{-7}	7.15×10^{-7}
$\tilde{\Gamma}_S$	2.17×10^{-6}	2.17×10^{-6}
Γ	1.55	1.54

TABLE VI. Helicity contributions and total decay widths, in units of 10^{-15} GeV, for the D_1 meson.

We have in this case the product of branching fractions

$$\begin{aligned} \mathcal{B}(B^+ \rightarrow \bar{D}'_1{}^0 l^+ \nu_l) \mathcal{B}(\bar{D}'_1{}^0 \rightarrow D^{*-} \pi^+) &= 1.32 \times 10^{-3}, \\ \mathcal{B}(B^0 \rightarrow D'_1{}^- l^+ \nu_l) \mathcal{B}(D'_1{}^- \rightarrow \bar{D}^{*0} \pi^-) &= 1.23 \times 10^{-3}. \end{aligned} \quad (42)$$

which are a rough factor of 2 smaller than the results from the BaBar Collaboration [2].

3. Semileptonic $B \rightarrow D_1(2420) l \nu_l$ decay

As in the previous case, the branching fraction $\mathcal{B}(D_1 \rightarrow D^* \pi^\pm)$ is again $2/3$ in our model because $D_1 \rightarrow D^* \pi$ is the only OZI-allowed decay channel.

Table VI shows the different helicity contributions to the semileptonic width of the reactions $B^+ \rightarrow \bar{D}_1^0 l^+ \nu_l$ and $B^0 \rightarrow D_1^- l^+ \nu_l$. The most important contribution is given by Γ_L . The ratio $\Gamma_L/\Gamma = 0.75$ gives the probability for the final D_1 meson to have helicity 0. This result is in agreement with the values $0.72 - 0.81$ obtained in the HQET calculation of Ref. [21].

Figure 3 shows the q^2 dependence of the form factors and the differential decay width for neutral D_1 channel, in panels (a) and (b), respectively. Again, a very similar result is obtained for the charged case.

The product of branching fractions are

$$\begin{aligned} \mathcal{B}(B^+ \rightarrow \bar{D}_1^0 l^+ \nu_l) \mathcal{B}(\bar{D}_1^0 \rightarrow D^{*-} \pi^+) &= 2.57 \times 10^{-3}, \\ \mathcal{B}(B^0 \rightarrow D_1^- l^+ \nu_l) \mathcal{B}(D_1^- \rightarrow \bar{D}^{*0} \pi^-) &= 2.39 \times 10^{-3}, \end{aligned} \quad (43)$$

which in this case compare very well with the latest BaBar data [3].

4. Semileptonic $B \rightarrow D_2^* l \nu_l$ decay

The semileptonic decay is studied by reconstructing the decay channel $D_2^* \rightarrow D^{(*)} \pi^-$, using the decay chain $D^* \rightarrow D^0 \pi$ for D^* meson and $D^0 \rightarrow K^- \pi^+$ or $D^+ \rightarrow K^- \pi^+ \pi^+$ for D meson. What is actually measured is the product of branching fractions $\mathcal{B}(B^+ \rightarrow \bar{D}_2^{*0} l^+ \nu_l) \mathcal{B}(\bar{D}_2^{*0} \rightarrow D^- \pi^+)$ and $\mathcal{B}(B^+ \rightarrow \bar{D}_2^{*0} l^+ \nu_l) \mathcal{B}(\bar{D}_2^{*0} \rightarrow D^{*-} \pi^+)$.

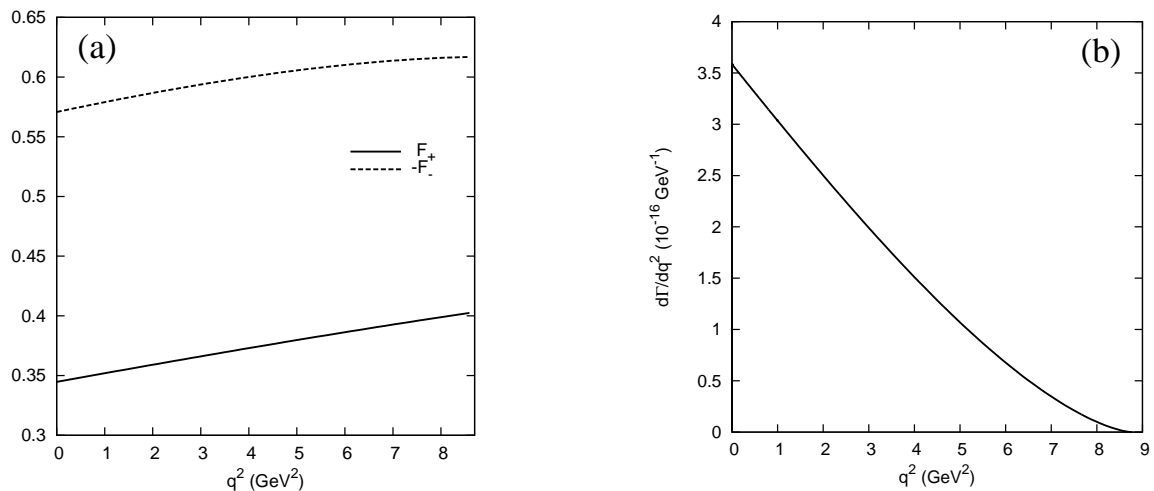


FIG. 1. Form factors and differential decay widths for the $B^+ \rightarrow \bar{D}_0^{*0} l^+ \nu_l$ decay as a function of q^2 . Very similar results are obtained for the $B^0 \rightarrow D_0^{*-} l^+ \nu_l$ decay. (a): Form factors predicted by CQM. (b): Differential decay width predicted by CQM.

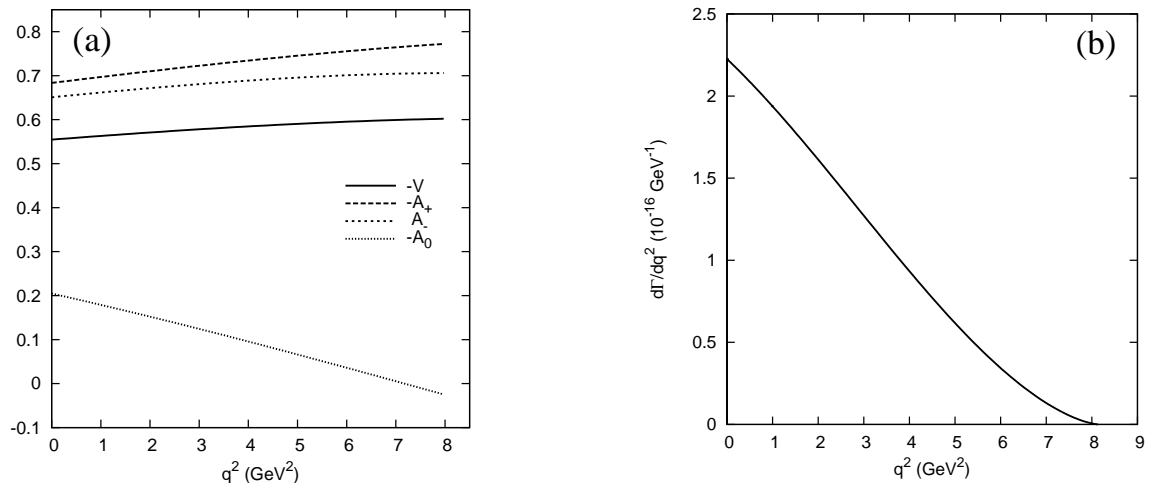


FIG. 2. Form factors and differential decay widths for the $B^+ \rightarrow \bar{D}_1^{\prime 0} l^+ \nu_l$ decay as a function of q^2 . Very similar results are obtained for the $B^0 \rightarrow D_1^{\prime -} l^+ \nu_l$ decay. (a): Form factors predicted by CQM. (b): Differential decay width predicted by CQM.

The first step of this decay involves a semileptonic process which can be calculated using Eq. (30). In Table VII we show the different helicity contributions to the total width. The main contribution is Γ_L in both neutral and charged D_2^* channels, providing almost 2/3 of the total width. The following one is Γ_U , the rest of the contributions being negligible. Again our ratio $\Gamma_L/\Gamma = 0.67$ is in agreement with the values 0.63 – 0.64 obtained in Ref. [21] using HQET.

Figure 4 shows the q^2 dependence in the form factors and in the differential decay width, panels (a) and (b) respectively, for the $B^+ \rightarrow \bar{D}_2^{*0} l^+ \nu_l$ decay. Very similar results (not shown) are obtained for the $B^0 \rightarrow D_2^{*-} l^+ \nu_l$

	$B^+ \rightarrow D_2^{*0} l^+ \nu_l$	$B^0 \rightarrow D_2^{*-} l^+ \nu_l$
Γ_U	0.44	0.44
$\tilde{\Gamma}_U$	2.56×10^{-8}	2.56×10^{-8}
Γ_L	0.90	0.91
$\tilde{\Gamma}_L$	5.27×10^{-7}	5.29×10^{-7}
$\tilde{\Gamma}_S$	1.54×10^{-6}	1.55×10^{-6}
Γ	1.34	1.35

TABLE VII. Helicity contributions and total decay widths, in units of 10^{-15} GeV, for the D_2^* meson.

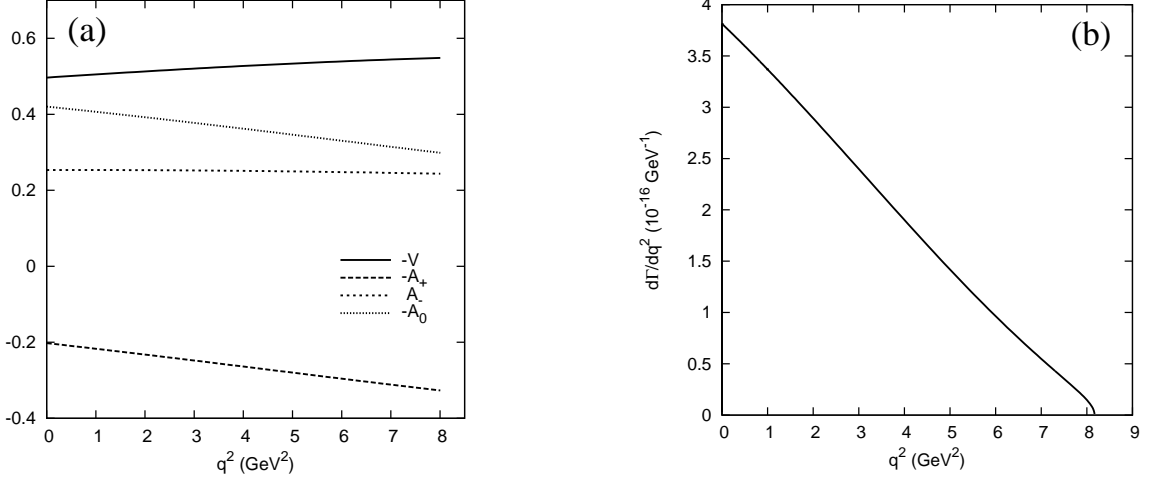


FIG. 3. Form factors and differential decay widths for the $B^+ \rightarrow D_1^0 l^+ \nu_l$ decay as a function of q^2 . The differences with respect $B^0 \rightarrow D_1^- l^+ \nu_l$ are negligible. (a): Form factors predicted by CQM. (b): Differential decay width predicted by CQM.

Branching ratio	Exp.	3P_0	Microscopic
$\Gamma(D^0 \pi^+)/\Gamma(D^{*0} \pi^+)$	$1.9 \pm 1.1 \pm 0.3$	1.80	1.97
$\Gamma(D^+ \pi^-)/\Gamma(D^{*+} \pi^-)$	1.56 ± 0.16	1.82	1.97
$\Gamma(D^+ \pi^-)/\Gamma(D^{(*)+} \pi^-)$	$0.62 \pm 0.03 \pm 0.02$	0.65	0.66

TABLE VIII. Branching ratios for D_2^* decays collected by the PDG [4] and our theoretical results calculated through the two strong decay models.

case.

The subsequent strong decays which appear are $D_2^* \rightarrow D^* \pi^-$ and $D_2^* \rightarrow D \pi^-$. In Table VIII we show the strong decay branching ratios obtained with the 3P_0 and microscopic models. They are in good agreement with experimental data [4].

Finally, we obtain the products of branching fractions for both decay chains considering that the total width of the D_2^* meson is the sum of the partial widths of $D^* \pi$ and $D \pi$ channels since these are the only OZI-allowed processes

$$\begin{aligned}
 \mathcal{B}(B^+ \rightarrow D_2^{*0} l^+ \nu_l) \mathcal{B}(D_2^{*0} \rightarrow D^+ \pi^-) &= \begin{cases} 1.44 \times 10^{-3} \\ 1.48 \times 10^{-3} \end{cases} \\
 \mathcal{B}(B^+ \rightarrow D_2^{*0} l^+ \nu_l) \mathcal{B}(D_2^{*0} \rightarrow D^{*+} \pi^-) &= \begin{cases} 0.79 \times 10^{-3} \\ 0.75 \times 10^{-3} \end{cases} \\
 \mathcal{B}(B^0 \rightarrow D_2^{*-} l^+ \nu_l) \mathcal{B}(D_2^{*-} \rightarrow D^0 \pi^-) &= \begin{cases} 1.34 \times 10^{-3} \\ 1.38 \times 10^{-3} \end{cases} \\
 \mathcal{B}(B^0 \rightarrow D_2^{*-} l^+ \nu_l) \mathcal{B}(D_2^{*-} \rightarrow D^{*0} \pi^-) &= \begin{cases} 0.74 \times 10^{-3} \\ 0.70 \times 10^{-3} \end{cases}
 \end{aligned} \tag{44}$$

where the first one refers to the calculation using the 3P_0

model and the second one comes from the microscopic model. These results are in very good agreement with BaBar data [3].

5. Summary of the results

Final results and their comparisons with the experimental data are given in Table IX. Except for the $D_1'(2430)$, the predictions are in very good agreement with the latest experimental measurements, Belle for $D_0(2400)$ and BaBar for $D_1(2420)$ and $D_2^*(2460)$. For the $D_1'(2430)$ there is also a strong disagreement between experimental data in the neutral case.

B. B_s semileptonic decays into D_s^{**} mesons

The semileptonic decays of B_s meson into orbitally excited P -wave charmed-strange mesons (D_s^{**}) provides an extra opportunity to get more insight into this system.

The $j_q = 1/2$ doublet, $D_{s0}^*(2318)$ and $D_{s1}(2460)$, shows surprisingly light masses which are below the DK and D^*K thresholds, respectively. These unexpected properties have triggered many theoretical interpretations, including four quark states, molecules, and the coupling of the $q\bar{q}$ components with different structures. As mentioned before, the $D_{s1}(2460)$ meson has an important non- $q\bar{q}$ contribution.

We have calculated the semileptonic B_s decays assuming that the D_s^{**} mesons are pure $q\bar{q}$ systems. For the $D_{s0}^*(2318)$ and $D_{s1}(2460)$, which are below the corresponding $D^{(*)}K$ thresholds, we only quote the weak decay branching fractions. Concerning the $D_{s1}(2460)$, and as shown in Ref. [15], the 1P_1 and 3P_1 probabilities

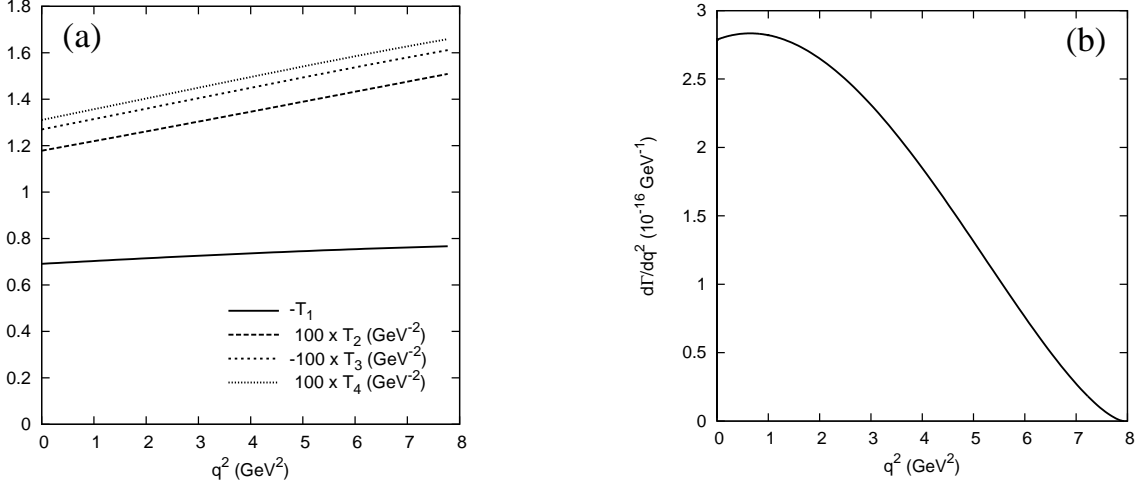


FIG. 4. Form factors and differential decay widths for the $B^+ \rightarrow D_2^{*0} l^+ \nu_l$ decay as a function of q^2 . Very similar results are obtained for the $B^0 \rightarrow D_2^{*-} l^+ \nu_l$ decay. (a): Form factors predicted by CQM. (b): Differential decay width predicted by CQM.

	Belle [1] ($\times 10^{-3}$)	BaBar [2, 3] ($\times 10^{-3}$)	3P_0 ($\times 10^{-3}$)	Mic. ($\times 10^{-3}$)
$D_0^*(2400)$				
$\mathcal{B}(B^+ \rightarrow \bar{D}_0^{*0} l^+ \nu_l) \mathcal{B}(\bar{D}_0^{*0} \rightarrow D^- \pi^+)$	$2.4 \pm 0.4 \pm 0.6$	$2.6 \pm 0.5 \pm 0.4$	2.15	2.15
$\mathcal{B}(B^0 \rightarrow D_0^{*-} l^+ \nu_l) \mathcal{B}(D_0^{*-} \rightarrow \bar{D}^0 \pi^-)$	$2.0 \pm 0.7 \pm 0.5$	$4.4 \pm 0.8 \pm 0.6$	1.80	1.80
$D_1'(2430)$				
$\mathcal{B}(B^+ \rightarrow \bar{D}_1'^0 l^+ \nu_l) \mathcal{B}(\bar{D}_1'^0 \rightarrow D^{*-} \pi^+)$	< 0.7	$2.7 \pm 0.4 \pm 0.5$	1.32	1.32
$\mathcal{B}(B^0 \rightarrow D_1'^- l^+ \nu_l) \mathcal{B}(D_1'^- \rightarrow \bar{D}^{*0} \pi^-)$	< 5	$3.1 \pm 0.7 \pm 0.5$	1.23	1.23
$D_1(2420)$				
$\mathcal{B}(B^+ \rightarrow \bar{D}_1^0 l^+ \nu_l) \mathcal{B}(\bar{D}_1^0 \rightarrow D^{*-} \pi^+)$	$4.2 \pm 0.7 \pm 0.7$	$2.97 \pm 0.17 \pm 0.17$	2.57	2.57
$\mathcal{B}(B^0 \rightarrow D_1^- l^+ \nu_l) \mathcal{B}(D_1^- \rightarrow \bar{D}^{*0} \pi^-)$	$5.4 \pm 1.9 \pm 0.9$	$2.78 \pm 0.24 \pm 0.25$	2.39	2.39
$D_2^*(2460)$				
$\mathcal{B}(B^+ \rightarrow \bar{D}_2^{*0} l^+ \nu_l) \mathcal{B}(\bar{D}_2^{*0} \rightarrow D^- \pi^+)$	$2.2 \pm 0.3 \pm 0.4$	$1.4 \pm 0.2 \pm 0.2^{(*)}$	1.43	1.47
$\mathcal{B}(B^+ \rightarrow \bar{D}_2^{*0} l^+ \nu_l) \mathcal{B}(\bar{D}_2^{*0} \rightarrow D^{*-} \pi^+)$	$1.8 \pm 0.6 \pm 0.3$	$0.9 \pm 0.2 \pm 0.2^{(*)}$	0.79	0.75
$\mathcal{B}(B^+ \rightarrow \bar{D}_2^{*0} l^+ \nu_l) \mathcal{B}(\bar{D}_2^{*0} \rightarrow D^{(*)-} \pi^+)$	$4.0 \pm 0.7 \pm 0.5$	$2.3 \pm 0.2 \pm 0.2$	2.22	2.22
$\mathcal{B}(B^0 \rightarrow D_2^{*-} l^+ \nu_l) \mathcal{B}(D_2^{*-} \rightarrow \bar{D}^0 \pi^-)$	$2.2 \pm 0.4 \pm 0.4$	$1.1 \pm 0.2 \pm 0.1^{(*)}$	1.34	1.38
$\mathcal{B}(B^0 \rightarrow D_2^{*-} l^+ \nu_l) \mathcal{B}(D_2^{*-} \rightarrow \bar{D}^{*0} \pi^-)$	< 3	$0.7 \pm 0.2 \pm 0.1^{(*)}$	0.74	0.70
$\mathcal{B}(B^0 \rightarrow D_2^{*-} l^+ \nu_l) \mathcal{B}(D_2^{*-} \rightarrow \bar{D}^{(*)0} \pi^-)$	< 5.2	$1.8 \pm 0.3 \pm 0.1$	2.08	2.08
$\mathcal{B}_{D/D^{(*)}}$	0.55 ± 0.03	$0.62 \pm 0.03 \pm 0.02$	0.65	0.66

TABLE IX. Most recent experimental measurements reported by Belle and BaBar Collaborations and their comparison with our results. The symbol (*) indicates the estimated results from the original data using $B_{D/D^{(*)}}$.

change with the coupling to non- $q\bar{q}$ degrees of freedom. What we do here is to vary these probabilities (including the phase) in order to obtain the limits of the decay width in the case of the $D_{s1}(2460)$ being a pure $q\bar{q}$ state, see Fig. 5. Assuming that non- $q\bar{q}$ components will give a small contribution to the weak decay, experimental results lower than these limits will be an indication of a

more complex structure for this meson.

For the decay into $D_{s1}(2536)$, our model predicts the weak decay branching fraction $\mathcal{B}(B_s^0 \rightarrow D_{s1}(2536)\mu^+\nu_\mu) = 4.77 \times 10^{-3}$ and the strong branching fractions $\mathcal{B}(D_{s1}(2536)^- \rightarrow D^{*-} \bar{K}^0) = 0.43$ (0.47) for the 3P_0 (microscopic) models. The final result appears in Table X. It is in good agreement with the existing

	Experiment ($\times 10^{-3}$)	Theory ($\times 10^{-3}$)
$D_{s0}^*(2318)$		
$\mathcal{B}(B_s^0 \rightarrow D_{s0}^*(2318)^- \mu^+ \nu_\mu)$	-	4.43
$D_{s1}(2460)$		
$\mathcal{B}(B_s^0 \rightarrow D_{s1}(2460)^- \mu^+ \nu_\mu)$	-	1.74 – 5.70
$D_{s1}(2536)$		3P_0 Mic.
$\mathcal{B}(B_s^0 \rightarrow D_{s1}(2536)^- \mu^+ \nu_\mu) \mathcal{B}(D_{s1}(2536)^- \rightarrow D^{*-} \bar{K}^0)$	2.4 ± 0.7 [4, 5]	2.05 2.24
$D_{s2}^*(2573)$		3P_0 Mic.
$\mathcal{B}(B_s^0 \rightarrow D_{s2}^*(2573)^- \mu^+ \nu_\mu) \mathcal{B}(D_{s2}^*(2573)^- \rightarrow D^- \bar{K}^0)$	-	1.70 1.77
$\mathcal{B}(B_s^0 \rightarrow D_{s2}^*(2573)^- \mu^+ \nu_\mu) \mathcal{B}(D_{s2}^*(2573)^- \rightarrow D^{*-} \bar{K}^0)$	-	0.18 0.11
$\mathcal{B}(B_s^0 \rightarrow D_{s2}^*(2573)^- \mu^+ \nu_\mu) \mathcal{B}(D_{s2}^*(2573)^- \rightarrow D^{(*)-} \bar{K}^0)$	-	1.88 1.88

TABLE X. Our predictions and their comparison with the available experimental data for semileptonic B_s decays into orbitally excited charmed-strange mesons.

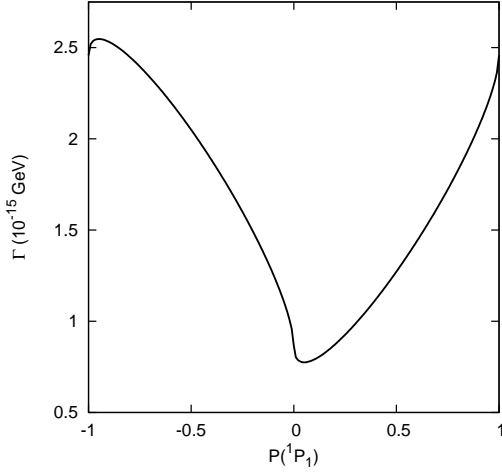


FIG. 5. Decay width for the $B_s^0 \rightarrow D_{s1}(2460)^- \mu^+ \nu_\mu$ decay as a function of the 1P_1 component probability. The sign reflects the relative phase between 1P_1 and 3P_1 components: -1 opposite phase and +1 same phase.

experimental data [4], which to us is a confirmation of our former result in Ref. [15] about the $q\bar{q}$ nature of this state.

In the case of the $D_{s2}^*(2573)$ the open strong decays are DK and D^*K , so the experimental measurements must be referred to $\mathcal{B}(B_s^0 \rightarrow D_{s2}^*(2573)^- \mu^+ \nu_\mu) \mathcal{B}(D_{s2}^*(2573)^- \rightarrow D^- \bar{K}^0)$ and $\mathcal{B}(B_s^0 \rightarrow D_{s2}^*(2573)^- \mu^+ \nu_\mu) \mathcal{B}(D_{s2}^*(2573)^- \rightarrow D^{*-} \bar{K}^0)$.

For the weak branching fraction we get in this case $\mathcal{B}(B_s^0 \rightarrow D_{s2}^*(2573)^- \mu^+ \nu_\mu) = 3.76 \times 10^{-3}$. For the strong

decay part of the reaction, we obtain in our model

$$\begin{aligned} \mathcal{B}(D_{s2}^{*-} \rightarrow D^- \bar{K}^0) &= \begin{cases} 0.45 \\ 0.47, \end{cases} \\ \mathcal{B}(D_{s2}^{*-} \rightarrow D^{*-} \bar{K}^0) &= \begin{cases} 0.047 \\ 0.030, \end{cases} \end{aligned} \quad (45)$$

where the first one refers to the calculation using the 3P_0 model and the second one comes from the microscopic model. Our final results can be seen in Table. X.

Besides we predict the ratio

$$\frac{\Gamma(D_{s2}^* \rightarrow DK)}{\Gamma(D_{s2}^* \rightarrow DK) + \Gamma(D_{s2}^* \rightarrow D^*K)} = \begin{cases} 0.91 & {}^3P_0 \\ 0.94 & \text{Mic.} \end{cases} \quad (46)$$

VI. CONCLUSIONS

We have performed a calculation of the branching fractions for the semileptonic decays of B and B_s mesons into final states containing orbitally excited charmed and charmed-strange mesons, respectively.

We worked in the framework of the constituent quark model of Ref. [10]. The model parameters were fitted to the meson spectra in Refs. [10, 14]. Our meson states are close to the ones predicted by HQS as expected.

We have calculated the semileptonic decay rates within the helicity formalism of Ref. [22] and following the work in Ref. [23]. The strong decay widths have been calculated using two models, the 3P_0 model and a microscopic model based on the quark-antiquark interactions present in the CQM model of Ref. [10].

From the experimental point of view, Belle and BaBar Collaborations provide their most recent measurements for the B meson in Refs. [1] and [2, 3] respectively. For the B_s meson only the product of branching fractions

$\mathcal{B}(B_s^0 \rightarrow D_{s1}(2536)^-\mu^+\nu_\mu)\mathcal{B}(D_{s1}(2536)^- \rightarrow D^{*-}\bar{K}^0)$ has been determined [4] using the experimental data on $\mathcal{B}(\bar{b} \rightarrow B_s^0)\mathcal{B}(B_s^0 \rightarrow D_{s1}(2536)^-\mu^+\nu_\mu)\mathcal{B}(D_{s1}(2536)^- \rightarrow D^{*-}\bar{K}^0)$ measured by the D0 Collaboration [5] and the PDG's best value for $\mathcal{B}(\bar{b} \rightarrow B_s^0)$ [4].

Our results for B semileptonic decays into $D_0^*(2400)$, $D_1(2420)$ and $D_2(2460)$ are in good agreement with the latest experimental measurements. In the case of $D_1'(2430)$ the prediction lies a factor of 2 below BaBar data. Note however the disagreement between BaBar and Belle data for the neutral case.

In the case of B_s semileptonic decays, our prediction for the $\mathcal{B}(B_s^0 \rightarrow D_{s1}(2536)^-\mu^+\nu_\mu)\mathcal{B}(D_{s1}(2536)^- \rightarrow D^{*-}\bar{K}^0)$ product of branching fractions is in agreement with the experimental data. This, together with the properties calculated in Ref. [15], is to us evidence of

a dominant $q\bar{q}$ structure for the $D_{s1}(2536)$ meson. We also give predictions for decays into other D_s^{**} mesons which can be useful to test the $q\bar{q}$ nature of these states.

ACKNOWLEDGMENTS

This work has been partially funded by the Spanish Ministerio de Ciencia y Tecnología under Contracts Nos. FIS2006-03438, FIS2009-07238 and FPA2010-21750-C02-02, by the Spanish Ingenio-Consolider 2010 Programs CPAN CSD2007-00042 and MultiDark CSD2009-0064, and by the European Community-Research Infrastructure Integrating Activity 'Study of Strongly Interacting Matter' (HadronPhysics2 Grant No. 227431). C. A. thanks a Juan de la Cierva contract from the Spanish Ministerio de Educación y Ciencia.

Appendix A: Form factor decomposition of hadronic matrix elements

Here we give general expressions valid for transitions between a pseudoscalar meson M_I at rest with quark content $\bar{q}_{f_1}q_{f_2}$ and a final M_F meson with total angular momentum and parity $J^P = 0^+, 1^+, 2^+$, three-momentum $-|\vec{q}|\vec{k}$, and quark content $\bar{q}_{f_1'}q_{f_2}$. The transition changes the antiquark flavor. Following Ref. [23] we evaluate $V_\lambda^\mu(|\vec{q}|)$ and $A_\lambda^\mu(|\vec{q}|)$ in the CQM through the relations

$$\begin{aligned} V_\lambda^\mu(|\vec{q}|) &= \sqrt{2m_I 2E_F(-\vec{q})} {}_{NR}\langle M_F, \lambda - |\vec{q}|\vec{k} | J_V^{bc\mu}(0) | M_I, \vec{0} \rangle_{NR} \\ A_\lambda^\mu(|\vec{q}|) &= \sqrt{2m_I 2E_F(-\vec{q})} {}_{NR}\langle M_F, \lambda - |\vec{q}|\vec{k} | J_A^{bc\mu}(0) | M_I, \vec{0} \rangle_{NR} \end{aligned} \quad (\text{A1})$$

For the different cases under study we will have the following.

1. Case $0^- \rightarrow 0^+$

$$\begin{aligned} A^0(|\vec{q}|) &= \sqrt{2m_I 2E_F(-\vec{q})} \int d^3p \frac{1}{4\pi|\vec{p}|} \left(\hat{\phi}_{f_1'f_2}^{(M(0^+))}(|\vec{p}|) \right)^* \hat{\phi}_{f_1f_2}^{(M(0^-))} \left(\vec{p} - \frac{m_{f_2}}{m_{f_1'} + m_{f_2}} q\vec{k} \right) \\ &\quad \sqrt{\frac{\hat{E}_{f_1'}\hat{E}_{f_1}}{4E_{f_1'}E_{f_1}}} \left[\frac{\vec{p} \cdot \left(\frac{m_{f_2}}{m_{f_1'} + m_{f_2}} |\vec{q}|\vec{k} - \vec{p} \right)}{\hat{E}_{f_1}} + \frac{\vec{p} \cdot \left(-\frac{m_{f_1'}}{m_{f_1'} + m_{f_2}} |\vec{q}|\vec{k} - \vec{p} \right)}{\hat{E}_{f_1}} \right], \\ A^3(|\vec{q}|) &= \sqrt{2m_I 2E_F(-\vec{q})} \\ &\quad \times \int d^3p \frac{1}{4\pi|\vec{p}|} \left(\hat{\phi}_{f_1'f_2}^{(M(0^+))}(|\vec{p}|) \right)^* \hat{\phi}_{f_1f_2}^{(M(0^-))} \left(\vec{p} - \frac{m_{f_2}}{m_{f_1'} + m_{f_2}} q\vec{k} \right) \sqrt{\frac{\hat{E}_{f_1'}\hat{E}_{f_1}}{4E_{f_1'}E_{f_1}}} \\ &\quad \times \left\{ p_z \left(1 - \frac{\left(-\frac{m_{f_1'}}{m_{f_1'} + m_{f_2}} |\vec{q}|\vec{k} - \vec{p} \right) \cdot \left(\frac{m_{f_2}}{m_{f_1'} + m_{f_2}} |\vec{q}|\vec{k} - \vec{p} \right)}{\hat{E}_{f_1'}\hat{E}_{f_1}} \right) + \frac{1}{\hat{E}_{f_1'}\hat{E}_{f_1}} \left[\left(-\frac{m_{f_1'}}{m_{f_1'} + m_{f_2}} |\vec{q}| - p_z \right) \right. \right. \\ &\quad \left. \left. \times \vec{p} \cdot \left(\frac{m_{f_2}}{m_{f_1'} + m_{f_2}} |\vec{q}|\vec{k} - \vec{p} \right) + \left(\frac{m_{f_2}}{m_{f_1'} + m_{f_2}} |\vec{q}| - p_z \right) \vec{p} \cdot \left(-\frac{m_{f_1'}}{m_{f_1'} + m_{f_2}} |\vec{q}|\vec{k} - \vec{p} \right) \right] \right\}. \end{aligned} \quad (\text{A2})$$

$E_{f'_1}$ and E_{f_1} are shorthand notations for $E_{f'_1}(-\frac{m_{f'_1}}{m_{f'_1}+m_{f_2}}|\vec{q}|\vec{k}-\vec{p})$ and $E_{f_1}(\frac{m_{f_2}}{m_{f'_1}+m_{f_2}}|\vec{q}|\vec{k}-\vec{p})$ respectively and $\hat{E}_f = E_f + m_f$.

2. Case $0^- \rightarrow 1^+$

Here we have to distinguish two different cases that depend on the total spin S of the quark-antiquark system.

i) Case $S = 0$

$$\begin{aligned}
V_{\lambda=0}^{(1^+, S=0)0}(|\vec{q}|) &= -i\sqrt{3}\sqrt{2m_I 2E_F(-\vec{q})} \int d^3p \sqrt{\frac{\hat{E}_{f'_1}\hat{E}_{f_1}}{4E_{f'_1}E_{f_1}}} \frac{1}{4\pi p} \left(\hat{\phi}_{f'_1 f_2}^{(M_F(1^+, S=0))}(p) \right)^* \\
&\quad \times \hat{\phi}_{f_1 f_2}^{(M_I(0^-))}(|\vec{p}-\frac{m_{f_2}}{m_{f'_1}+m_{f_2}}|\vec{q}|\vec{k}|) p_z \left[1 + \frac{\left(-\frac{m_{f'_1}}{m_{f'_1}+m_{f_2}}|\vec{q}|\vec{k}-\vec{p} \right) \cdot \left(\frac{m_{f_2}}{m_{f'_1}+m_{f_2}}|\vec{q}|\vec{k}-\vec{p} \right)}{\hat{E}_{f_1}\hat{E}_{f_1}} \right], \\
V_{\lambda=-1}^{(1^+, S=0)1}(|\vec{q}|) &= i\sqrt{\frac{3}{2}}\sqrt{2m_I 2E_F(-\vec{q})} \int d^3p \sqrt{\frac{\hat{E}_{f'_1}\hat{E}_{f_1}}{4E_{f'_1}E_{f_1}}} \frac{1}{4\pi p} \left(\hat{\phi}_{f'_1 f_2}^{(M_F(1^+, S=0))}(p) \right)^* \\
&\quad \times \hat{\phi}_{f_1 f_2}^{(M_I(0^-))}(|\vec{p}-\frac{m_{f_2}}{m_{f'_1}+m_{f_2}}|\vec{q}|\vec{k}|) p_x^2 \left(\frac{1}{\hat{E}_{f_1}} + \frac{1}{\hat{E}_{f'_1}} \right), \\
V_{\lambda=0}^{(1^+, S=0)3}(|\vec{q}|) &= -i\sqrt{3}\sqrt{2m_I 2E_F(-\vec{q})} \int d^3p \sqrt{\frac{\hat{E}_{f'_1}\hat{E}_{f_1}}{4E_{f'_1}E_{f_1}}} \frac{1}{4\pi p} \left(\hat{\phi}_{f'_1 f_2}^{(M_F(1^+, S=0))}(p) \right)^* \\
&\quad \times \hat{\phi}_{f_1 f_2}^{(M_I(0^-))}(|\vec{p}-\frac{m_{f_2}}{m_{f'_1}+m_{f_2}}|\vec{q}|\vec{k}|) p_z \left(\frac{\frac{m_{f_2}}{m_{f'_1}+m_{f_2}}|\vec{q}|-p_z}{\hat{E}_{f_1}} - \frac{\frac{m_{f'_1}}{m_{f'_1}+m_{f_2}}|\vec{q}|-p_z}{\hat{E}_{f'_1}} \right), \\
A_{\lambda=-1}^{(1^+, S=0)1}(|\vec{q}|) &= -i\sqrt{\frac{3}{2}}\sqrt{2m_I 2E_F(-\vec{q})} \int d^3p \sqrt{\frac{\hat{E}_{f'_1}\hat{E}_{f_1}}{4E_{f'_1}E_{f_1}}} \frac{1}{4\pi p} \left(\hat{\phi}_{f'_1 f_2}^{(M_F(1^+, S=0))}(p) \right)^* \\
&\quad \times \hat{\phi}_{f_1 f_2}^{(M_I(0^-))}(|\vec{p}-\frac{m_{f_2}}{m_{f'_1}+m_{f_2}}|\vec{q}|\vec{k}|) \frac{p_y^2|\vec{q}|}{\hat{E}_{f_1}\hat{E}_{f'_1}}. \tag{A3}
\end{aligned}$$

ii) Case $S = 1$

$$\begin{aligned}
V_{\lambda=0}^{(1^+, S=1)0}(|\vec{q}|) &= i\sqrt{\frac{3}{2}}\sqrt{2m_I 2E_F(-\vec{q})} \int d^3p \sqrt{\frac{\hat{E}_{f'_1} \hat{E}_{f_1}}{4E_{f'_1} E_{f_1}}} \frac{1}{4\pi p} \left(\hat{\phi}_{f'_1 f_2}^{(M_F(1^+, S=1))}(p) \right)^* \\
&\quad \times \hat{\phi}_{f'_1 f_2}^{(M_I(0^-))} \left(|\vec{p} - \frac{m_{f_2}}{m_{f'_1} + m_{f_2}} |\vec{q}| \vec{k} | \right) \frac{|\vec{q}|(p_z^2 - p^2)}{\hat{E}_{f'_1} \hat{E}_{f_1}}, \\
V_{\lambda=-1}^{(1^+, S=1)1}(|\vec{q}|) &= -i\frac{\sqrt{3}}{2}\sqrt{2m_I 2E_F(-\vec{q})} \int d^3p \sqrt{\frac{\hat{E}_{f'_1} \hat{E}_{f_1}}{4E_{f'_1} E_{f_1}}} \frac{1}{4\pi p} \left(\hat{\phi}_{f'_1 f_2}^{(M_F(1^+, S=1))}(p) \right)^* \\
&\quad \times \hat{\phi}_{f'_1 f_2}^{(M_I(0^-))} \left(|\vec{p} - \frac{m_{f_2}}{m_{f'_1} + m_{f_2}} |\vec{q}| \vec{k} | \right) \left(\frac{p_y^2 + p_z^2 + p_z |\vec{q}| \frac{m_{f'_1}}{m_{f'_1} + m_{f_2}}}{\hat{E}_{f'_1}} - \frac{p_y^2 + p_z^2 - p_z |\vec{q}| \frac{m_{f_2}}{m_{f'_1} + m_{f_2}}}{\hat{E}_{f_1}} \right), \\
V_{\lambda=0}^{(1^+, S=1)3}(|\vec{q}|) &= i\sqrt{\frac{3}{2}}\sqrt{2m_I 2E_F(-\vec{q})} \int d^3p \sqrt{\frac{\hat{E}_{f'_1} \hat{E}_{f_1}}{4E_{f'_1} E_{f_1}}} \frac{1}{4\pi p} \left(\hat{\phi}_{f'_1 f_2}^{(M_F(1^+, S=1))}(p) \right)^* \\
&\quad \times \hat{\phi}_{f'_1 f_2}^{(M_I(0^-))} \left(|\vec{p} - \frac{m_{f_2}}{m_{f'_1} + m_{f_2}} |\vec{q}| \vec{k} | \right) (p_x^2 + p_y^2) \left(\frac{1}{\hat{E}_{f_1}} - \frac{1}{\hat{E}_{f'_1}} \right), \\
A_{\lambda=-1}^{(1^+, S=1)1}(|\vec{q}|) &= i\frac{\sqrt{3}}{2}\sqrt{2m_I 2E_F(-\vec{q})} \\
&\quad \int d^3p \sqrt{\frac{\hat{E}_{f'_1} \hat{E}_{f_1}}{4E_{f'_1} E_{f_1}}} \frac{1}{4\pi p} \left(\hat{\phi}_{f'_1 f_2}^{(M_F(1^+, S=1))}(p) \right)^* \hat{\phi}_{f'_1 f_2}^{(M_I(0^-))} \left(|\vec{p} - \frac{m_{f_2}}{m_{f'_1} + m_{f_2}} |\vec{q}| \vec{k} | \right) \\
&\quad \times \left\{ p_z \left[1 - \frac{\left(-\frac{m_{f'_1}}{m_{f'_1} + m_{f_2}} |\vec{q}| \vec{k} - \vec{p} \right) \cdot \left(\frac{m_{f_2}}{m_{f'_1} + m_{f_2}} |\vec{q}| \vec{k} - \vec{p} \right)}{\hat{E}_{f'_1} \hat{E}_{f_1}} \right] + \frac{m_{f_2} - m_{f'_1}}{m_{f'_1} + m_{f_2}} \frac{p_x^2 |\vec{q}|}{\hat{E}_{f'_1} \hat{E}_{f_1}} \right\}. \tag{A4}
\end{aligned}$$

3. Case $0^- \rightarrow 2^+$

Here we have to distinguish between $L = 1$ and $L = 3$.

i) Case $L = 1$

$$\begin{aligned}
V_{\lambda=+1}^{(2^+, L=1)1}(|\vec{q}|) &= -i \frac{\sqrt{3}}{2} \sqrt{2m_I 2E_F(-\vec{q})} \int d^3p \sqrt{\frac{\hat{E}_{f'_1} \hat{E}_{f_1}}{4E_{f'_1} E_{f_1}}} \frac{1}{4\pi p} \left(\hat{\phi}_{f'_1 f_2}^{(M_F(2^+, L=1))}(p) \right)^* \\
&\quad \times \hat{\phi}_{f_1 f_2}^{(M_I(0^-))} \left(|\vec{p} - \frac{m_{f_2}}{m_{f'_1} + m_{f_2}} |\vec{q}| \vec{k} | \right) \left(\frac{p_y^2 - p_z^2 - p_z |\vec{q}| \frac{m_{f'_1}}{m_{f'_1} + m_{f_2}}}{\hat{E}_{f'_1}} - \frac{p_y^2 - p_z^2 + p_z |\vec{q}| \frac{m_{f_2}}{m_{f'_1} + m_{f_2}}}{\hat{E}_{f_1}} \right), \\
A_{\lambda=0}^{(2^+, L=1)0}(|\vec{q}|) &= -\frac{i}{\sqrt{2}} \sqrt{2m_I 2E_F(-\vec{q})} \int d^3p \sqrt{\frac{\hat{E}_{f'_1} \hat{E}_{f_1}}{4E_{f'_1} E_{f_1}}} \frac{1}{4\pi p} \left(\hat{\phi}_{f'_1 f_2}^{(M_F(2^+, L=1))}(p) \right)^* \\
&\quad \times \hat{\phi}_{f_1 f_2}^{(M_I(0^-))} \left(|\vec{p} - \frac{m_{f_2}}{m_{f'_1} + m_{f_2}} |\vec{q}| \vec{k} | \right) \left(\frac{p_x^2 + p_y^2 - 2p_z^2 - 2p_z |\vec{q}| \frac{m_{f'_1}}{m_{f'_1} + m_{f_2}}}{\hat{E}_{f'_1}} \right. \\
&\quad \left. + \frac{p_x^2 + p_y^2 - 2p_z^2 + 2p_z |\vec{q}| \frac{m_{f_2}}{m_{f'_1} + m_{f_2}}}{\hat{E}_{f_1}} \right), \\
A_{\lambda=+1}^{(2^+, L=1)1}(|\vec{q}|) &= i \frac{\sqrt{3}}{2} \sqrt{2m_I 2E_F(-\vec{q})} \int d^3p \sqrt{\frac{\hat{E}_{f'_1} \hat{E}_{f_1}}{4E_{f'_1} E_{f_1}}} \frac{1}{4\pi p} \left(\hat{\phi}_{f'_1 f_2}^{(M_F(2^+, L=1))}(p) \right)^* \\
&\quad \times \hat{\phi}_{f_1 f_2}^{(M_I(0^-))} \left(|\vec{p} - \frac{m_{f_2}}{m_{f'_1} + m_{f_2}} |\vec{q}| \vec{k} | \right) \left\{ p_z \left[1 - \frac{\left(-\frac{m_{f'_1}}{m_{f'_1} + m_{f_2}} |\vec{q}| \vec{k} - \vec{p} \right) \cdot \left(\frac{m_{f_2}}{m_{f'_1} + m_{f_2}} |\vec{q}| \vec{k} - \vec{p} \right)}{\hat{E}_{f'_1} \hat{E}_{f_1}} \right] \right. \\
&\quad \left. + \frac{4p_z p_x^2 - p_x^2 |\vec{q}| \frac{m_{f_2} - m_{f'_1}}{m_{f'_1} + m_{f_2}}}{\hat{E}_{f'_1} \hat{E}_{f_1}} \right\}, \\
A_{\lambda=0}^{(2^+, L=1)3}(|\vec{q}|) &= -i \sqrt{2} \sqrt{2m_I 2E_F(-\vec{q})} \int d^3p \sqrt{\frac{\hat{E}_{f'_1} \hat{E}_{f_1}}{4E_{f'_1} E_{f_1}}} \frac{1}{4\pi p} \left(\hat{\phi}_{f'_1 f_2}^{(M_F(2^+, L=1))}(p) \right)^* \\
&\quad \times \hat{\phi}_{f_1 f_2}^{(M_I(0^-))} \left(|\vec{p} - \frac{m_{f_2}}{m_{f'_1} + m_{f_2}} |\vec{q}| \vec{k} | \right) \left\{ p_z \left[1 - \frac{\left(-\frac{m_{f'_1}}{m_{f'_1} + m_{f_2}} |\vec{q}| \vec{k} - \vec{p} \right) \cdot \left(\frac{m_{f_2}}{m_{f'_1} + m_{f_2}} |\vec{q}| \vec{k} - \vec{p} \right)}{\hat{E}_{f'_1} \hat{E}_{f_1}} \right] \right. \\
&\quad + \frac{1}{\hat{E}_{f'_1} \hat{E}_{f_1}} \left[2p_z \left(-\frac{m_{f'_1}}{m_{f'_1} + m_{f_2}} |\vec{q}| - p_z \right) \left(\frac{m_{f_2}}{m_{f'_1} + m_{f_2}} |\vec{q}| - p_z \right) + \right. \\
&\quad \left. \left. (p_x^2 + p_y^2) \left(-p_z + \frac{m_{f_2} - m_{f'_1}}{2(m_{f'_1} + m_{f_2})} |\vec{q}| \right) \right] \right\}. \tag{A5}
\end{aligned}$$

ii) Case $L = 3$

$$\begin{aligned}
V_{\lambda=+1}^{(2^+, L=3)1}(|\vec{q}|) &= \frac{i}{\sqrt{8}} \sqrt{2m_I 2E_F(-\vec{q})} \int d^3p \sqrt{\frac{\hat{E}_{f'_1} \hat{E}_{f_1}}{4E_{f'_1} E_{f_1}}} \frac{1}{4\pi p^3} \left(\hat{\phi}_{f'_1 f_2}^{(M(2^+, L=3))}(p) \right)^* \\
&\quad \times \hat{\phi}_{f_1 f_2}^{(M(0^-))} \left(|\vec{p} - \frac{m_{f_2}}{m_{f'_1} + m_{f_2}} |\vec{q}| \vec{k} \right) \\
&\quad \times \left[\frac{1}{\hat{E}_{f_1}} \left(p^2 \left(2p_y^2 - 3p_z \left(\frac{m_{f_2}}{m_{f'_1} + m_{f_2}} |\vec{q}| - p_z \right) \right) \right. \right. \\
&\quad \left. \left. + 5p_z \left(-2p_y^2 p_z + \left(\frac{m_{f_2}}{m_{f'_1} + m_{f_2}} |\vec{q}| - p_z \right) (p_x^2 - p_y^2 + p_z^2) \right) \right) \right. \\
&\quad \left. + \frac{1}{\hat{E}_{f'_1}} \left(p^2 \left(-2p_y^2 + 3p_z \left(-\frac{m_{f'_1}}{m_{f'_1} + m_{f_2}} |\vec{q}| - p_z \right) \right) \right. \right. \\
&\quad \left. \left. - 5p_z \left(-2p_y^2 p_z + \left(-\frac{m_{f'_1}}{m_{f'_1} + m_{f_2}} |\vec{q}| - p_z \right) (p_x^2 - p_y^2 + p_z^2) \right) \right) \right], \\
A_{T\lambda=0}^{(2^+, L=3)0}(|\vec{q}|) &= -i \sqrt{\frac{3}{4}} \sqrt{2m_I 2E_F(-\vec{q})} \int d^3p \sqrt{\frac{\hat{E}_{f'_1} \hat{E}_{f_1}}{4E_{f'_1} E_{f_1}}} \frac{1}{4\pi p} \left(\hat{\phi}_{f'_1 f_2}^{(M(2^+, L=3))}(p) \right)^* \\
&\quad \times \hat{\phi}_{f_1 f_2}^{(M(0^-))} \left(|\vec{p} - \frac{m_{f_2}}{m_{f'_1} + m_{f_2}} |\vec{q}| \vec{k} \right) \left[\left(\frac{5p_z^2}{p^2} - 1 \right) \left(\frac{p_x^2 + p_y^2}{\hat{E}_{f_1}} + \frac{p_x^2 + p_y^2}{\hat{E}_{f'_1}} \right) \right. \\
&\quad \left. - \frac{p_z}{p} \left(\frac{5p_z^2}{p^2} - 3 \right) \left(\frac{\frac{m_{f_2}}{m_{f'_1} + m_{f_2}} |\vec{q}| - p_z}{\hat{E}_{f_1}} - \frac{\frac{m_{f'_1}}{m_{f'_1} + m_{f_2}} |\vec{q}| + p_z}{\hat{E}_{f'_1}} \right) \right], \\
A_{\lambda=0}^{(2^+, L=3)3}(|\vec{q}|) &= -\frac{i}{2} \sqrt{2m_I 2E_F(-\vec{q})} \int d^3p \sqrt{\frac{\hat{E}_{f'_1} \hat{E}_{f_1}}{4E_{f'_1} E_{f_1}}} \frac{1}{4\pi p} \left(\hat{\phi}_{f'_1 f_2}^{(M(2^+, L=3))}(p) \right)^* \\
&\quad \times \hat{\phi}_{f_1 f_2}^{(M(0^-))} \left(|\vec{p} - \frac{m_{f_2}}{m_{f'_1} + m_{f_2}} |\vec{q}| \vec{k} \right) \left[(p_x^2 + p_y^2) \left(\frac{5p_z^2}{p^2} - 1 \right) \left(\frac{\frac{m_{f_2} - m_{f'_1}}{m_{f'_1} + m_{f_2}} |\vec{q}| - 2p_z}{\hat{E}_{f_1} \hat{E}_{f'_1}} \right) \right. \\
&\quad \left. - p_z \left(\frac{5p_z^2}{p^2} - 3 \right) \left(1 - \frac{p_x^2 + p_y^2 - \left(-\frac{m_{f'_1}}{m_{f'_1} + m_{f_2}} |\vec{q}| - p_z \right) \left(\frac{m_{f_2}}{m_{f'_1} + m_{f_2}} |\vec{q}| - p_z \right)}{\hat{E}_{f_1} \hat{E}_{f'_1}} \right) \right], \\
A_{\lambda=+1}^{(2^+, L=3)1}(|\vec{q}|) &= -\frac{i}{\sqrt{8}} \sqrt{2m_I 2E_F(-\vec{q})} \int d^3p \sqrt{\frac{\hat{E}_{f'_1} \hat{E}_{f_1}}{4E_{f'_1} E_{f_1}}} \frac{1}{4\pi p} \left(\hat{\phi}_{f'_1 f_2}^{(M(2^+, L=3))}(p) \right)^* \\
&\quad \times \hat{\phi}_{f_1 f_2}^{(M(0^-))} \left(|\vec{p} - \frac{m_{f_2}}{m_{f'_1} + m_{f_2}} |\vec{q}| \vec{k} \right) \left[3p_z \right. \\
&\quad \left. + 3p_z \frac{p_x^2 - p_y^2 - \left(-\frac{m_{f'_1}}{m_{f'_1} + m_{f_2}} |\vec{q}| - p_z \right) \left(\frac{m_{f_2}}{m_{f'_1} + m_{f_2}} |\vec{q}| - p_z \right)}{\hat{E}_{f_1} \hat{E}_{f'_1}} \right. \\
&\quad \left. + 5p_z \left(\frac{p_x^2}{p^2} + \frac{p_y^2}{p^2} - \frac{p_z^2}{p^2} \right) \left(1 + \frac{p_x^2 - p_y^2 - \left(-\frac{m_{f'_1}}{m_{f'_1} + m_{f_2}} |\vec{q}| - p_z \right) \left(\frac{m_{f_2}}{m_{f'_1} + m_{f_2}} |\vec{q}| - p_z \right)}{\hat{E}_{f_1} \hat{E}_{f'_1}} \right) \right. \\
&\quad \left. - 2p_x^2 \left(\frac{5p_z^2}{p^2} - 1 \right) \left(\frac{\frac{m_{f_2} - m_{f'_1}}{m_{f'_1} + m_{f_2}} |\vec{q}| - 2p_z}{\hat{E}_{f_1} \hat{E}_{f'_1}} \right) + 20 \frac{p_z p_x^2 p_y^2}{\hat{E}_{f_1} \hat{E}_{f'_1} p^2} \right].
\end{aligned}$$

- [1] D. Liventsev *et al.* (Belle Collaboration), Phys. Rev. D **77**, 091503 (2008).
- [2] B. Aubert *et al.* (BaBar Collaboration), Phys. Rev. Lett. **101**, 261802 (2008).
- [3] B. Aubert *et al.* (BaBar Collaboration), Phys. Rev. Lett. **103**, 051803 (2009).
- [4] K. Nakamura *et al.* (Particle Data Group), J. Phys. G **37**, 075021 (2010).
- [5] V.M. Abazov *et al.* (D0 Collaboration), Phys. Rev. Lett. **102**, 051801 (2009).
- [6] L. Micu, Nucl. Phys. B **10**, 521 (1969).
- [7] R. Kokoski and N. Isgur, Phys. Rev. D **35**, 907 (1987).
- [8] E. Eichten, K. Gottfried, T. Kinoshita, K.D. Lane and T. M. Yan, Phys. Rev. D **17**, 3090 (1978); *ibid.* **21**, 203 (1980).
- [9] E.S. Ackleh, T. Barnes and E.S. Swanson, Phys. Rev. D **54**, 6811 (1996).
- [10] J. Vijande, F. Fernández and A. Valcarce, J. Phys. G **31**, 481 (2005).
- [11] H. Garcilazo, A. Valcarce and F. Fernández, Phys. Rev. C **63**, 035207 (2001); Phys. Rev. C **64**, 058201 (2001).
- [12] J. Vijande, H. Garcilazo, A. Valcarce and F. Fernández, Phys. Rev. D **70**, 054022 (2004).
- [13] F. Fernández, A. Valcarce, P. González and V. Vento, Phys. Lett. B **287**, 35 (1992).
- [14] J. Segovia, A.M. Yasser, D.R. Entem and F. Fernández, Phys. Rev. D **78**, 114033 (2008).
- [15] J. Segovia, A.M. Yasser, D.R. Entem and F. Fernández, Phys. Rev. D **80**, 054017 (2009).
- [16] D. Diakonov, Prog. Part. Nucl. Phys. **51**, 173 (2003).
- [17] M.D. Scadron Phys. Rev. D **26**, 239 (1982).
- [18] G.S. Bali *et al.*, Phys. Rev. D **71**, 114513 (2005).
- [19] E. Hiyama, Y. Kino, and M. Kamimura, Prog. Part. Nucl. Phys. **51**, 223 (2003).
- [20] A. K. Leibovich, Z. Ligeti, I. W. Stewart and M. B. Wise, Phys. Rev. Lett. **78**, 3995 (1997).
- [21] A. K. Leibovich, Z. Ligeti, I. W. Stewart and M. B. Wise, Phys. Rev. D **57**, 308 (1998).
- [22] M.A. Ivanov, J.G. Körner and P. Santorelli, Phys. Rev. D **73**, 054024 (2006).
- [23] E. Hernández, J. Nieves and J.M. Verde-Velasco, Phys. Rev. D **74**, 074008 (2006).
- [24] A. Le Yaouanc, L. Oliver, O. Pène and J. Raynal, Phys. Rev. D **8**, 2223 (1973); **9**, 1415 (1974); **11**, 1272 (1975).
- [25] J. Segovia, D.R. Entem and F. Fernández, in progress.
- [26] R. Bonnaz and B. Silvestre-Brac, Few-Body Syst. **27**, 163 (1999).
- [27] N. Isgur and M.B. Wise, Phys. Rev. Lett. **66**, 1130 (1991).